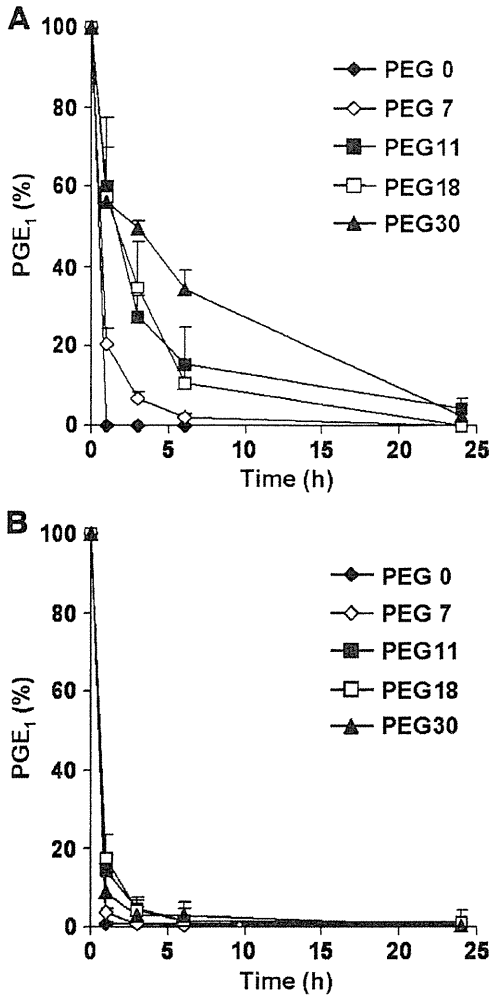

Fig. 2. The effect of PEG content of PLA-nanoparticles on their clearance from the circulation and on induction of the ABC phenomenon. **A** Various types of nanoparticles (PEG0, PEG7, PEG11, PEG18 and PEG30 (NP-L20)) were prepared as described in the legend of Tables I and II. Rats were intravenously administered PEG0, PEG7, PEG11, PEG18 or PEG30 (133 μg PGE_1/kg). Plasma PGE_1 levels were monitored and are shown as described in the legend of Fig. 1. Values are mean ± S.E.M. (n=3–4) **B** Rats were intravenously administered PEG0, PEG7, PEG11, PEG18 or PEG30 (50 μg nanoparticles/rat). After 7 days, the same type of nanoparticles (1,000 μg nanoparticles/rat) was administered and the amount of PGE_1 in plasma was monitored and shown as described above. Values are mean ± S.E.M. (n=3–6).

induced IgM antibodies recognize PEG rather than PLA, as reported for PEGylated liposomes (11).

Effect of the PEG Content of Nanoparticles on Induction of the ABC Phenomenon

It was reported that PEG content in PEGylated liposomes affects induction of the ABC phenomenon (36). Here we prepared PGE_1-encapsulated nanoparticles in the presence of various ratios of PLA and PEG-PLA (PEG30 means the nanoparticles prepared in the presence of 30% PEG (w/w); the real content of PEG in the prepared nanoparticles is shown in Table I). The particle size and the efficiency of encapsulation (PGE_1 content in nanoparticles) were similar for these types of nanoparticles (PEG0, PEG7, PEG11, PEG18 and PEG30), except that the particle size of PEG0 was larger than other types of nanoparticles (Table I).

We first examined the blood clearance profiles of the various types of nanoparticles following their intravenous injection into naïve rats in an attempt to understand their stealth effects. As shown in Fig. 2A, more rapid clearance from the circulation was observed with nanoparticles with lower PEG content, confirming that PEG confers the stealth effect of PLA-nanoparticles. Pharmacokinetic parameters ($AUC_{(0-24)}$ and CL) support this notion: approximately, $AUC_{(0-24)}$ became higher but CL became lower with the increase in the PEG content of nanoparticles (Table II). We then examined induction of the ABC phenomenon by these types of nanoparticles in a manner similar to the experiment summarized in Fig. 1A. Injection of a second dose of each of any of the types of nanoparticles at the time interval of 7 days resulted in very rapid clearance from the circulation (Fig. 2B). To evaluate the ABC phenomenon, we calculated the ratio of $AUC_{(0-24)}$ for the second injection (Fig. 2B) to that of the first one (Fig. 2A) as the ABC index; a value of 1 for this index means no induction of the ABC phenomenon. As shown in Table II, the ABC indexes for all types of nanoparticles except PEG0 were less than 1, and there is no apparent relationship between PEG content and the ABC index, showing that PEG-modified PLA-nanoparticles induce the ABC phenomenon irrespective of their PEG content. Based on the results in Fig. 2 and Table I, we fixed the PEG content at 30% because this achieved a good stealth effect, and we tried to find another way to suppress the ABC phenomenon.

Effect of Particle Size and Molecular Weight of PLA in Nanoparticles on Induction of the ABC Phenomenon

For PEGylated liposomes, it was reported that their size and physicochemical properties affect their ability to induce the ABC phenomenon (8). We have also reported that use of L-PLA of higher molecular weight improves the sustained-release profile of PGE_1 from nanoparticles (4). Thus, we prepared various types of nanoparticles with different diameters and compositions (NP-L20s, NP-L33 and NP-L33s). NP-L33 and NP-L33s were prepared from L-PLA (Mw=28,100), and NP-L20s and NP-L33s have a smaller particle size than NP-L20 and NP-L33 (Table III). The efficiency of encapsulation of PGE_1 was lower in nanoparticles with smaller size or

Table II. Characteristics of PGE_1-Encapsulated PLA-nanoparticles Containing Different Amounts of PEG

Codes	$AUC_{(0-24)}$ (μg·h/ml)	CL (ml/h·kg)	ABC index
PEG 0	0.39±0.13	401.0±97.7	1.43±0.14
PEG 7	0.93±0.07	143.9±10.5	0.53±0.02
PEG11	3.22±0.66	45.5±10.4	0.24±0.04
PEG18	2.98±0.51	47.9±9.8	0.41±0.08
PEG30	6.34±0.58	21.5±2.0	0.20±0.04

Pharmacokinetic parameters were calculated by moment analysis of the results shown in Fig. 2A. The ABC index was calculated as follows: ABC index = AUC of the second dose (Fig. 2B)/AUC of the first dose (Fig. 2A). Values are mean ± S.E.M. (n=4).

Table III. Characteristics of Various PGE_1-Encapsulated Nanoparticles with Different Diameters and Compositions

Codes	L-PLA Mw (kDa)	PEG content (%)	PGE_1 content (%)	Particle size (nm)
NP-L20	17.5	23.7±1.2	1.11±0.10	119±2
NP-L20s	17.5	28.7±1.8	0.86±0.04	81±6
NP-L33	28.1	30.4±0.8	0.83±0.17	134±4
NP-L33s	28.1	23.8±1.6	0.20±0.01	69±2

Nanoparticles encapsulating PGE_1 were prepared with 13 mg L-PLA (Mw=17 500) or L-PLA (Mw=28 100) and 12 mg PEG-D,L-PLA in the presence of 5 mg PGE_1, 1.2 mg iron chloride and 4.8 mg DEA by an oil-in-water solvent diffusion method. The nanoparticles were characterized as described in the legend of Tables I and II. Values are given as mean ± S.E.M. (n=3).

in those prepared from longer L-PLA (Table III). As a result, the PGE_1 content of NP-L33s was less than one-fifth of that of NP-L20 (Table III). At first, we compared the induction of anti-PEG IgM antibody after injection of these types of nanoparticles. As shown in Fig. 3A, compared to NP-L20, NP-L33s induced anti-PEG IgM antibody production to a lesser extent: the maximum level was lower and the level returned to the original level more rapidly. In addition, the induction of anti-PEG IgM antibody by NP-L20s or NP-L33 was less apparent than that by NP-L20; however, the difference was not as apparent as for NP-L33s (Fig. 3A).

We then examined induction of the ABC phenomenon by the various types of nanoparticles. As well as NP-L20, NP-L20s and NP-L33 gave rise to the ABC phenomenon when the second dose was injected at day 7 or 14 after injection of the first dose. However, they induced the phenomenon to a lesser extent than NP-L20 (Fig. 3B and Table IV). In contrast, NP-L33s did not exhibit the ABC phenomenon when the second dose was injected at day 14 after the first injection (Fig. 3B and Table IV). The ABC phenomenon was not apparent for any of the nanoparticles when the second dose was injected at day 28 after the injection of first dose (Fig. 3B and Table IV). The results for the ABC phenomenon shown in Fig. 3B correlate well with the induction of anti-PEG IgM antibody production shown in Fig. 3A, supporting the notion that anti-PEG IgM antibody is responsible for the ABC phenomenon. The results in Fig. 3B also show that NP-L33s has the better stealth effect than NP-L20 (Table IV).

Release Profile of PGE_1 from Nanoparticles *In Vitro*

Considering the clinical setting, the time interval of repeated injections of PGE_1-encapsulated nanoparticles could be prolonged with improvement of the sustained-release profile of PGE_1. Thus, we examined the release profile of PGE_1 from the NP-L20, NP-L20s, NP-L33 and NP-L33s upon incubation at 37°C in 50% fetal bovine serum (FBS) *in vitro* (Fig. 4). Since the concentration of PGE_1 in the medium (i.e. released PGE_1) was below the limits of detection in the preliminary experiment, the amount released was determined by measuring the PGE_1 remaining in the particles. We separated the nanoparticles from the medium by centrifugation (69,000 g for 30 min).

As shown in Fig. 4, NP-L20 showed a release profile similar to that observed in a previous paper (4) and more than half of the encapsulated PGE_1 was released from NP-L20 within 14 days. As suggested in previous reports (37,38), use of PLA with higher molecular weight resulted in a better sustained-release profile (Fig. 4). Furthermore, although the underlying mechanism is unknown, NP-L20s and NP-L33s showed better sustained-release profiles than NP-L20 and NP-L33, respectively (Fig. 4). This result is surprising, because it is generally believed that drug release from smaller size particles is faster due to the higher surface area. One possible explanation is that the distribution of PGE_1 in nanoparticles is not uniform and this distribution is affected by size of nanoparticles. Nevertheless, NP-L33s showed the best sustained-release profile, and more than half of the encapsulated PGE_1 remained in NP-L33s even after incubation for 28 days. These results suggest that NP-L33s is beneficial, not only because it results in less ABC phenomenon-inducing activity but also because it exhibits a better sustained-release profile of encapsulated PGE_1.

DISCUSSION

In order to develop a new formulation of PGE_1 that enables targeting and sustained-release drug delivery, we incorporated PGE_1 into PEG-modified PLA-nanoparticles (4). Before applying this formulation to a clinical setting, it is necessary to test whether it induces the ABC phenomenon, because this phenomenon may decrease the therapeutic efficacy of an encapsulated drug upon repeated administration. Consequently, in this study, we found that the ABC phenomenon is induced by the PEG-modified PLA-nanoparticles. Furthermore, we examined the mechanism underlying this phenomenon and could develop modified PGE_1-encapsulated nanoparticles that are less active in inducing the ABC phenomenon and show a better sustained release profile for encapsulated PGE_1.

The ABC phenomenon was identified for PEGylated liposomes, and its mechanism has been studied extensively for these liposomes (8). It was recently reported that the ABC phenomenon can also be induced by polymeric micelles (39,40). Here we have shown that the phenomenon can be induced by PEG-modified PLA nanoparticles, suggesting that the phenomenon is induced not specifically by PEGylated liposomes but generally by PEG-modified nanoparticles. Although it was reported that production of anti-PEG IgM antibody is induced by PEG-modified proteins in humans (41), it is not clear whether the ABC phenomenon is induced in humans. However, this possibility should be considered when PEG-modified nanoparticles are applied clinically in repeated intravenous administration.

Here we have examined which factors (time interval, dose, PEG content, molecular weight of PLA and particle size) affect induction of the ABC phenomenon by PEG-modified PLA-nanoparticles, referring to results for PEGy-

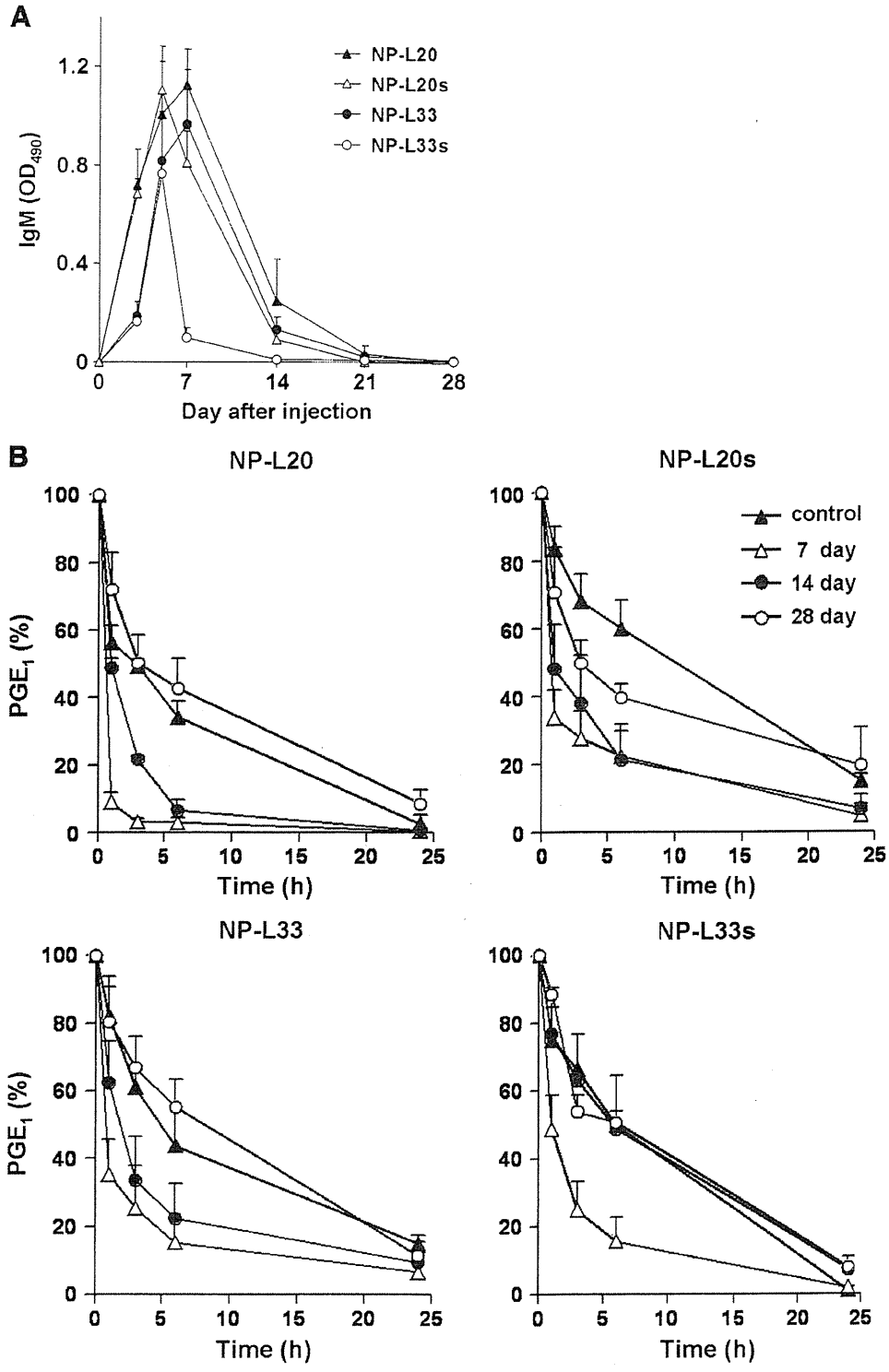

Fig. 3. Effect of molecular weight of L-PLA and particle size on induction of the ABC phenomenon and production of IgM antibody. **A** Various types of nanoparticles (NP-L20, NP-L20s, NP-L33 and NP-L33s) were prepared as described in the legend of Tables III and IV. Rats were intravenously administered each type of nanoparticle (50 μg nanoparticles/rat), and blood samples were taken periodically. The amount of anti-PEG IgM antibody was determined as described in the legend of Fig. 1. The NP-L20 data are the same as those in Fig. 1B. Values are mean ± S.E.M. (n=3–4). **B** Rats were intravenously administered each type of nanoparticle (50 μg nanoparticles/rat). At days 7, 14 or 28 days after the first injection, the same type of nanoparticles (1,000 μg nanoparticles/rat) was administered and the plasma PGE_1 levels were monitored and shown as described in the legend of Fig. 1. As a control, changes in plasma PGE_1 levels after the administration of each type of nanoparticles to naïve rats are shown. Values are mean ± S.E.M. (n=3–7).

Table IV. Characteristics of Various PGE_1-Encapsulated Nanoparticles with Different Diameters and Compositions

Codes	$AUC_{(0-24)}$ (μg·h/ml)	CL (ml/h·kg)	ABC index		
			7 day	14 day	28 day
NP-L20	6.35±0.58	21.5±2.0	0.17±0.03	0.39±0.04	1.26±0.25
NP-L20s	8.11±0.72	16.8±1.3	0.40±0.12	0.45±0.17	0.80±0.13
NP-L33	6.55±1.24	21.6±3.4	0.42±0.17	0.60±0.22	1.19±0.16
NP-L33s	7.59±0.76	18.0±1.8	0.43±0.12	1.06±0.19	1.07±0.05

Pharmacokinetic parameters were calculated based on the results shown in Fig. 3. The results were analysed as described in the legend of Tables I and II. Values are shown as mean ± S.E.M. (n=4).

lated liposomes. The time interval between injections clearly affected the ABC phenomenon: repeated injection of PEG-modified PLA-nanoparticles with a time interval of 7 days showed strongest induction of the phenomenon. Similar results were obtained for PEGylated liposomes (14). Doses (data not shown) or PEG content (Fig. 2) of the nanoparticles that were initially injected did not affect induction of the ABC phenomenon within the ranges of 1–1,000 μg PLA-nanoparticles (0.002–0.2 μmol PLA/kg) or 7–30% PEG content, respectively. Doses of the nanoparticles injected did not affect induction of the anti-PEG IgM antibodies within the ranges of 1–1,000 μg nanoparticles (data not shown). It was reported that a strong inverse relationship between the dose of initially injected PEGylated liposomes and the extent of the ABC phenomenon within the range of 0.001–5 μmol phospholipid/kg was observed and that PEG density beyond 5% suppressed induction of the ABC phenomenon (36). Thus, the effects of dose and PEG content of the initially injected nanoparticles on induction of the ABC phenomenon seem to differ depending on the types of nanoparticles. Smaller PEG-modified PLA-nanoparticles tended to induce the phenomenon to a lesser extent, which is in contrast to results observed for PEGylated liposomes (9). We also found that nanoparticles prepared from L-PLA (Mw=28,100) are less active for induction of the ABC phenomenon than those derived from L-PLA (Mw=17,500).

As for the mechanism for induction of the ABC phenomenon by PEG-modified PLA-nanoparticles, we suggest that anti-PEG IgM antibodies play an important role. The reason for this is that induction of anti-PEG IgM antibody by the first dose of nanoparticles and the magnitude of the ABC phenomenon observed after the second dose was generally well correlated. As pointed out for PEGylated liposomes (6,11,14–18), anti-PEG IgM antibodies induced by the first dose of PEG-modified PLA-nanoparticles may activate the complement system and opsonization by C3 fragments on the second dose, resulting in their uptake by MPS. However, the amount of anti-PEG IgM antibody did not completely correlate with the level of ABC phenomenon, as described above. Thus, a mechanism other than induction of production of anti-PEG IgM antibody may also be involved in this ABC phenomenon for PEG-modified PLA-nanoparticles.

Considering the potential clinical application of PGE_1-encapsulated PEG-modified PLA-nanoparticles, factors other than the ABC phenomenon (such as stealth effects and sustained-release profile) are also important. From this point of view, we propose that NP-L33s may be clinically beneficial as a targeted and sustained-release formulation of PGE_1 based on the following results from this study: (i) NP-L33s caused the weakest induction of production of anti-PEG IgM antibody and ABC phenomenon of the various types of nanoparticles, and no apparent ABC phenomenon was observed when these nanoparticles were repeatedly injected at an interval of 14 days; (ii) NP-L33s showed good stealth effect; (iii) NP-L33s showed the best sustained-release profile *in vitro*, and more than half of the encapsulated PGE_1 remained in the nanoparticles even after incubation for 28 days. Thus, if NP-L33s delivered to damaged blood vessels *in vivo* shows a similar sustained-release profile, it might keep the desired level of PGE_1 around the vessels upon repeated injection of once per 2 weeks or once per month without induction of the ABC phenomenon. However, since the optimum time interval for induction of the ABC phenomenon differs depending on the animal species for PEGylated liposomes (8,13), induction of the ABC phenomenon by NP-L33s in humans also needs to be examined.

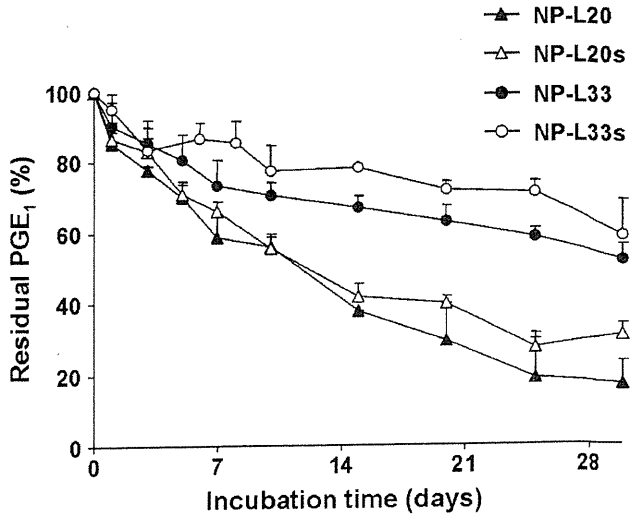

Fig. 4. Release profile of PGE_1 from nanoparticles *in vitro*. Various types of nanoparticles (NP-L20, NP-L20s, NP-L33 and NP-L33s) were prepared as described in the legend of Tables III and IV. Nanoparticles (at a particle concentration of 10 mg/ml) were dispersed in 50% FBS in PBS (*v/v*, 100 μl) and incubated at 37°C for the indicated periods. The PGE_1 content remaining in the nanoparticles as a function of time was determined by HPLC. Values shown are mean ± S.E.M. (n=6).

CONCLUSION

Based on the results of this study, we conclude that NP-L33s has a lower propensity than NP-L20 to induce the ABC phenomenon and a good sustained-release profile of PGE_1, which may be clinically useful.

ACKNOWLEDGEMENTS

This work was supported by Grants-in-Aid for Scientific Research from the Ministry of Health, Labour, and Welfare of Japan, as well as the Japan Science and Technology Agency and Grants-in-Aid for Scientific Research from the Ministry of Education, Culture, Sports, Science and Technology, Japan.

REFERENCES

1. Maeda H, Wu J, Sawa T, Matsumura Y, Hori K. Tumor vascular permeability and the EPR effect in macromolecular therapeutics: a review. J Control Release. 2000;65:271–84.
2. Gref R, Minamitake Y, Peracchia MT, Trubetskoy V, Torchilin V, Langer R. Biodegradable long-circulating polymeric nanospheres. Science 1994;263:1600–3.
3. Stolnik S, Dunn SE, Garnett MC, Davies MC, Coombes AG, Taylor DC, *et al.* Surface modification of poly(lactide-co-glycolide) nanospheres by biodegradable poly(lactide)-poly(ethylene glycol) copolymers. Pharm Res. 1994;11:1800–8.
4. Ishihara T, Takahashi M, Higaki M, Takenaga M, Mizushima T, Mizushima Y. Prolonging the *in vivo* residence time of prostaglandin E(1) with biodegradable nanoparticles. Pharm Res. 2008;25:1686–95.
5. Sharpe M, Easthope SE, Keating GM, Lamb HM. Polyethylene glycol-liposomal doxorubicin: a review of its use in the management of solid and haematological malignancies and AIDS-related Kaposi's sarcoma. Drugs 2002;62:2089–126.
6. Dams ET, Laverman P, Oyen WJ, Storm G, Scherphof GL, van Der Meer JW, *et al.* Accelerated blood clearance and altered biodistribution of repeated injections of sterically stabilized liposomes. J Pharmacol Exp Ther. 2000;292:1071–9.
7. Ishida T, Maeda R, Ichihara M, Mukai Y, Motoki Y, Manabe Y, *et al.* The accelerated clearance on repeated injection of pegylated liposomes in rats: laboratory and histopathological study. Cell Mol Biol Lett. 2002;7:286.
8. Ishida T, Kiwada H. Accelerated blood clearance (ABC) phenomenon upon repeated injection of PEGylated liposomes. Int J Pharm. 2008;354:56–62.
9. Wang XY, Ishida T, Ichihara M, Kiwada H. Influence of the physicochemical properties of liposomes on the accelerated blood clearance phenomenon in rats. J Control Release. 2005;104:91–102.
10. Laverman P, Carstens MG, Boerman OC, Dams ET, Oyen WJ, van Rooijen N, *et al.* Factors affecting the accelerated blood clearance of polyethylene glycol-liposomes upon repeated injection. J Pharmacol Exp Ther. 2001;298:607–12.
11. Ishida T, Ichihara M, Wang X, Yamamoto K, Kimura J, Majima E, *et al.* Injection of PEGylated liposomes in rats elicits PEG-specific IgM, which is responsible for rapid elimination of a second dose of PEGylated liposomes. J Control Release. 2006;112:15–25.
12. Ishida T, Atobe K, Wang X, Kiwada H. Accelerated blood clearance of PEGylated liposomes upon repeated injections: effect of doxorubicin-encapsulation and high-dose first injection. J Control Release. 2006;115:251–8.
13. Ishida T, Masuda K, Ichikawa T, Ichihara M, Irimura K, Kiwada H. Accelerated clearance of a second injection of PEGylated liposomes in mice. Int J Pharm. 2003;255:167–74.
14. Ishida T, Maeda R, Ichihara M, Irimura K, Kiwada H. Accelerated clearance of PEGylated liposomes in rats after repeated injections. J Control Release. 2003;88:35–42.
15. Wang X, Ishida T, Kiwada H. Anti-PEG IgM elicited by injection of liposomes is involved in the enhanced blood clearance of a subsequent dose of PEGylated liposomes. J Control Release. 2007;119:236–44.
16. Ishida T, Ichihara M, Wang X, Kiwada H. Spleen plays an important role in the induction of accelerated blood clearance of PEGylated liposomes. J Control Release. 2006;115:243–50.
17. Ishida T, Wang X, Shimizu T, Nawata K, Kiwada H. PEGylated liposomes elicit an anti-PEG IgM response in a T cell-independent manner. J Control Release. 2007;122:349–55.
18. Ishida T, Kashima S, Kiwada H. The contribution of phagocytic activity of liver macrophages to the accelerated blood clearance (ABC) phenomenon of PEGylated liposomes in rats. J Control Release. 2008;126:162–5.
19. Caro J, Migliaccio-Walle K, Ishak KJ, Proskorovsky I. The morbidity and mortality following a diagnosis of peripheral arterial disease: long-term follow-up of a large database. BMC Cardiovasc Disord. 2005;5:14.
20. Chandra Sekhar N. Effect of eight prostaglandins on platelet aggregation. J Med Chem. 1970;13:39–44.
21. Simmet T, Peskar BA. Prostaglandin E1 and arterial occlusive disease: pharmacological considerations. Eur J Clin Invest. 1988;18:549–54.
22. Carlson LA, Olsson AG. Intravenous prostaglandin E1 in severe peripheral vascular disease. Lancet. 1976;2:810.
23. Belch JJ, Bell PR, Creissen D, Dormandy JA, Kester RC, McCollum RD, *et al.* Randomized, double-blind, placebo-controlled study evaluating the efficacy and safety of AS-013, a prostaglandin E1 prodrug, in patients with intermittent claudication. Circulation 1997;95:2298–302.
24. Ferreira SH, Vane JR. Prostaglandins: their disappearance from and release into the circulation. Nature 1967;216:868–73.
25. Golub M, Zia P, Matsuno M, Horton R. Metabolism of prostaglandins A1 and E1 in man. J Clin Invest. 1975;56:1404–10.
26. Monkhouse DC, Van Campen L, Aguiar AJ. Kinetics of dehydration and isomerization of prostaglandins E 1 and E 2. J Pharm Sci. 1973;62:576–80.
27. Mizushima Y, Yanagawa A, Hoshi K. Prostaglandin E1 is more effective, when incorporated in lipid microspheres, for treatment of peripheral vascular diseases in man. J Pharm Pharmacol. 1983;35:666–7.
28. Mizushima Y. Lipo-prostaglandin preparations. Prostaglandins Leukot Essent Fatty Acids. 1991;42:1–6.
29. Mizushima Y. Lipid microspheres as novel drug carriers. Drugs Exp Clin Res. 1985;11:595–600.
30. Mizushima Y, Hamano T, Haramoto S, Kiyokawa S, Yanagawa A, Nakura K, *et al.* Distribution of lipid microspheres incorporating prostaglandin E1 to vascular lesions. Prostaglandins Leukot Essent Fatty Acids. 1990;41:269–72.
31. Igarashi R, Mizushima Y, Takenaga M, Matsumoto K, Morizawa Y, Yasuda A. A stable PGE1 prodrug for targeting therapy. J Control Release. 1992;20:37–46.
32. Yoshida T, Uetake A, Yamaguchi H, Nimura N, Kinoshita T. New preparation method for 9-anthryldiazomethane (ADAM) as a fluorescent labeling reagent for fatty acids and derivatives. Anal Biochem. 1988;173:70–4.
33. Ishihara T, Takahashi M, Higaki M, Mizushima Y. Efficient encapsulation of a water-soluble corticosteroid in biodegradable nanoparticles. Int J Pharm. 2009;365:200–5.
34. Ishihara T, Izumo N, Higaki M, Shimada E, Hagi T, Mine L, *et al.* Role of zinc in formulation of PLGA/PLA nanoparticles encapsulating betamethasone phosphate and its release profile. J Control Release. 2005;105:68–76.
35. Bazile D, Prud'homme C, Bassoullet MT, Marlard M, Spenlehauer G, Veillard M. Stealth Me.PEG-PLA nanoparticles avoid uptake by the mononuclear phagocytes system. J Pharm Sci. 1995; 84:493–8.
36. Ishida T, Harada M, Wang XY, Ichihara M, Irimura K, Kiwada H. Accelerated blood clearance of PEGylated liposomes following preceding liposome injection: effects of lipid dose and PEG surface-density and chain length of the first-dose liposomes. J Control Release. 2005;105:305–17.
37. Lee SW, Chang DH, Shim MS, Kim BO, Kim SO, Seo MH. Ionically fixed polymeric nanoparticles as a novel drug carrier. Pharm Res. 2007;24:1508–16.

38. Musumeci T, Ventura CA, Giannone I, Ruozi B, Montenegro L, Pignatello R, *et al.* PLA/PLGA nanoparticles for sustained release of docetaxel. Int J Pharm. 2006;325:172–9.
39. Koide H, Asai T, Hatanaka K, Urakami T, Ishii T, Kenjo E, *et al.* Particle size-dependent triggering of accelerated blood clearance phenomenon. Int J Pharm. 2008;362:197–200.
40. Lu W, Wan J, She Z, Jiang X. Brain delivery property and accelerated blood clearance of cationic albumin conjugated pegylated nanoparticle. J Control Release. 2007;118:38–53.
41. Richter AW, Akerblom E. Polyethylene glycol reactive antibodies in man: titer distribution in allergic patients treated with monomethoxy polyethylene glycol modified allergens or placebo, and in healthy blood donors. Int Arch Allergy Appl Immunol. 1984;74:36–9.

Journal of Controlled Release 134 (2009) 18–25

Contents lists available at ScienceDirect

Journal of Controlled Release

journal homepage: www.elsevier.com/locate/jconrel

Oxaliplatin targeting to angiogenic vessels by PEGylated cationic liposomes suppresses the angiogenesis in a dorsal air sac mouse model

Amr Abu-Lila, Takuya Suzuki, Yusuke Doi, Tatsuhiro Ishida *, Hiroshi Kiwada

Department of Pharmacokinetics and Biopharmaceutics, Subdivision of Biopharmaceutical Sciences, Institute of Health Biosciences, The University of Tokushima, 1-78-1, Sho-machi, Tokushima 770-8505, Japan

ARTICLE INFO

Article history:
Received 24 June 2008
Accepted 23 October 2008
Available online 5 November 2008

Keywords:
Anti-angiogenic therapy
Anticancer drugs
Oxaliplatin
Cationic liposome
Dorsal air sac (DAS) model

ABSTRACT

Oxaliplatin (trans-l-diaminocyclohexane oxalatoplatinum, l-OHP) is a third-generation platinum analogue with proven anti-tumor activity against many tumor cell lines, however it does not show sufficient anti-tumor activity *in vivo* when used alone. In order to overcome this problem and to achieve an anti-angiogenic therapy with l-OHP, the drug was encapsulated into PEG-coated cationic liposomes, which were designed to target the newly formed vessels, and its anti-angiogenic activity was evaluated in an *in vivo* mouse dorsal air sac (DAS) assay. For the DAS assay, chambers filled with tumor cells were implanted underneath the dorsal skin. l-OHP encapsulated in PEG-coated cationic liposomes (5 mg/kg mice) was intravenously injected once on day 1, 2, 3 or 4 after chamber implantation. On the fifth day after chamber implantation, animals were sacrificed and tumor-angiogenesis was evaluated. Liposome-encapsulated l-OHP completely suppressed angiogenesis in the skin when it was administered day 3 after chamber implantation. Under similar experimental conditions, neither l-OHP encapsulated in PEG-coated neutral liposomes, nor free l-OHP, nor "empty" (no drug containing) PEG-coated cationic liposomes showed such strong suppressive effect. The present study suggests that the liposomal formulation of l-OHP, which targeted to angiogenic vessels, has a remarkable *in vivo* anti-angiogenic activity and the formulation may become a promising novel approach to achieve anti-angiogenic therapy.

1. Introduction

Oxaliplatin (l-OHP), a cisplatin derivative, is currently approved and marketed for second-line treatment of colorectal cancer [1,2]. It contains a bulky carrier ligand within its structure, and forms DNA adducts that more effectively inhibit DNA synthesis but are also generally considered to be more cytotoxic than adducts of either cisplatin or carboplatin [3,4]. Moreover, unlike cisplatin, it can inhibit RNA synthesis [5]. However, it has been reported that l-OHP showed a low anti-tumor activity *in vivo* when used alone [6,7]. This lower anti-tumor activity can be attributed to the high partitioning to erythrocytes and low accumulation in tumor tissues following intravenous administration. Therefore, there is an obvious need for the development of an effective way to overcome this problem. Liposomes were one of the first nanomolecular drug delivery systems to show increased delivery of small molecular weight anticancer drugs to solid tumors by altering the biodistribution of associated drugs [8,9].

Tumor angiogenesis is an essential mechanism for the adequate supply of nutrients, oxygen, growth factors and other substances to tumor cells [10–12]. Tumor angiogenesis is not a singular process; at least two types of angiogenesis are believed to contribute to vessel growth in tumors [13]. One process involves the stimulation of new blood vessel capillaries to sprout in the neighboring mature host vasculature [14,15], while the other involves the recruitment of circulating endothelial precursor cells from the bone marrow to promote neo-vascularization [16–19]. Tumor angiogenesis is mainly triggered by growth factors in the microenvironment such as vascular endothelial growth factor, (VEGF), basic fibroblast growth factor (bFGF) and the matrix metalloproteinases (MMPs) [20–22]. These factors are generally produced by the tumors themselves, by the surrounding tissue, or by infiltrating macrophages. Suppression of the angiogenesis process, leading to eradication of primary tumor cells and suppression of metastasis through the disruption of the metastatic pathway, became a promising strategy for treating solid tumors (anti-angiogenic therapy) [23–25].

To target cancer cells, nanomolecular drug delivery system including anticancer agents must first cross the vasculature and then travel through the interstitium. However, the delivery system, if targeted to tumor angiogenic vessels, has the advantage that, once in the blood stream, it should have direct access to the target endothelial

Abbreviations: bFGF, basic fibroblast growth factor; CHOL, cholesterol; DAS, dorsal air sac; DC-6-14, O,O'-ditetradecanoyl-N-(alpha-trimethyl ammonio acetyl) diethanolamine chloride; DiI, 1,1'-dioctadecyl-3,3,3',3'-tetramethylindocarbocyanine perchlorate; DMEM, Dulbecco's modified Eagle's medium; ECs, endothelial cells; FBS, fetal bovine serum; HSPC, hydrogenated soya phosphatidylcholine; l-OHP, oxaliplatin; mPEG2000-DSPE, 1,2-distearoyl-sn-glycero-3-phosphoethanolamine-*n*-[methoxy (polyethyleneglycol)-2000]; MMPs, matrix metalloproteinases; VEGF, vascular endothelial growth factor.

* Corresponding author. Tel./fax: +81 88 633 7260.
E-mail address: ishida@ph.tokushima-u.ac.jp (T. Ishida).

0168-3659/$ – see front matter © 2008 Elsevier B.V. All rights reserved.
doi:10.1016/j.jconrel.2008.10.018

cells in the solid tumors. It has been shown that cationic liposomes have a propensity for localizing in tumor vessels [13,26,27]. A recent study indicated that PEG-coated cationic liposomes associate with approximately 27 and 5% of vessel areas in tumors and normal tissues, respectively, in human and murine tumor models [28]. This property of selective targeting of cationic liposomes to tumor angiogenic vessels may promote the selective delivery of l-OHP to tumor endothelial cells and thus the development of chemotherapeutic strategies involving vascular targeting.

In this study we propose that the selective delivery of l-OHP to angiogenic vessels should improve its low anti-tumor activity, and more specifically achieve effective anti-angiogenic therapy. We here report the development of l-OHP-containing PEG-coated cationic liposomes and their accumulation in angiogenic vessels in a mouse dorsal air sac (DAS) model [29,30]. Finally, we investigated the anti-angiogenic effect of the preparation by using a mouse DAS model.

2. Materials and methods

2.1. Materials

Hydrogenated soya phosphatidylcholine (HSPC) and 1,2-distearoyl-sn-glycero-3-phosphoethanolamine-*n*-[methoxy (polyethyleneglycol)-2000] ($mPEG_{2000}$-DSPE) were generously donated by Nippon Oil and Fat (Tokyo, Japan). Oxaliplatin (l-OHP) was generously donated by Taiho Pharmaceutical Co. (Tokyo, Japan). Cholesterol (CHOL) and O,O'-ditetradecanoyl-N-(alpha-trimethyl ammonio acetyl) diethanolamine chloride (DC-6-14) were purchased from Wako Pure Chemical Co. Ltd (Osaka, Japan). 1,1'-dioctadecyl-3,3,3',3'-tetramethylindocarbocyanine perchlorate (Dil) was purchased from Invitrogen (OR, USA). All other reagents were of analytical grade.

2.2. Animals and tumor cell line

Male ddY mice, 5 weeks old, were purchased from Japan SLC (Shizuoka, Japan). The experimental animals were allowed free access to water and mouse chow, and were housed under controlled environmental conditions (constant temperature, humidity, and 12 h dark–light cycle). All animal experiments were evaluated and approved by the Animal and Ethics Review Committee of the University of Tokushima. The mouse melanoma cell line, B16BL6, was maintained in Dulbecco's modified Eagle's medium (DMEM) (Nissui Pharmaceutical Co. Ltd., Tokyo) supplemented with 10% heat-inactivated FBS (Japan Bioserum, Hiroshima, Japan), 10 mM L-glutamine, 100 units/ml penicillin and 100 μg/ml streptomycin in a 5% CO_2 air incubator at 37 °C. B16BL6 cell line was purchased from Cell Resource Center for Biomedical Research (Institute of Development, Aging and Cancer, Tohoku University).

2.3. Preparation of liposomes

Cationic liposomes modified with $mPEG_{2000}$-DSPE were composed of HSPC/CHOL/DC-6-14/$mPEG_{2000}$-DSPE (2/1/0.2/0.2 molar ratio). Neutral liposomes modified with $mPEG_{2000}$-DSPE were composed of HSPC/CHOL/$mPEG_{2000}$-DSPE (2/1/0.2 molar ratio). In the targeting experiments, 1 mol% of the fluorescent lipid membrane marker, Dil, was added to the lipid mixture. All liposomes were prepared using the reverse-phase evaporation method. Briefly, lipids (50 mmole) were dissolved in 6 ml of chloroform/diethyl ether (1:2 v/v) and then 2 ml of l-OHP solution (8 mg/ml) in 5% (w/v) dextrose was dropped into the lipid mixture to form w/o emulsion. For preparation of "empty" (no drug-containing) PEG-coated cationic liposomes, 5% dextrose solution was added instead of l-OHP solution. The volume ratio of the aqueous to the organic phase was maintained at 1:3. The emulsion was sonicated for 15 min and then the organic phase was removed to form liposomes by evaporation in a rotary evaporator at 40 °C under vacuum at 250 hPa for 1 h. The resulting liposomes were extruded through a polycarbonate membrane (200 nm pore size) using an extruder device (Lipex Biomembranes Inc., Canada) maintained at 65 °C to obtain liposomes of approximately 250 nm (homogeneous size). The phospholipid concentration was determined by a colorimetric assay [31]. Un-encapsulated free l-OHP was removed by dialyzing the resulting liposomes against 5% dextrose using a dialysis cassette (Slyde-A-Lyzer, 10000MWCO, PIERCE, Rockford, IL, USA). Encapsulated l-OHP was quantified using an atomic absorption photometer (Z-5700, Hitachi, Tokyo). The size and zeta potential of the liposomes were determined by using a NICOMP 370 HPL submicron particle analyzer (Particle Sizing System, CA, USA). Encapsulation efficiency of l-OHP was calculated by dividing the drug to lipid ratio after the dialysis by the initial drug to lipids ratio. Liposome suspensions were stored in glass vials at 4 °C for 4 weeks to assess their physical stabilities with respect to change in the size distribution. For the treatment with animal model, l-OHP formulations freshly prepared were used.

2.4. In vitro stability assay

l-OHP-containing liposomes (5 mmole lipids) were mixed with either 50% mouse plasma or 5% dextrose solution at a ratio of 1:9 (v/v). The l-OHP concentration in the mixture was 0.203 mg/ml for neutral liposome and 0.176 mg/ml for cationic liposome, respectively. The resulting suspension was incubated at either 37 or 4 °C. Aliquots (300–500 μl) were withdrawn at specified time points for the determination of l-OHP retention in the liposome. The l-OHP-containing liposomes were separated from the leaked drug by means of a Sepharose CL-4B column, which had been equilibrated with HEPES buffered saline (25 mM HEPES, 140 mM NaCl, pH 7.4). The amount of phospholipids and l-OHP in the liposome fractions were determined as described above. The retention of the drug in the prepared liposomes was calculated by dividing the drug to phospholipid ratio at indicated time point by the initial drug to phospholipid ratio.

2.5. Partitioning of l-OHP into erythrocytes

Either free l-OHP solution or l-OHP encapsulated in PEG-coated cationic liposomes was injected intravenously in mice. Blood was collected at 3 and 6 h post injection in the presence of anticoagulant (heparin) and centrifuged to obtain plasma and the precipitate containing erythrocytes (erythrocytes fraction). l-OHP in plasma and erythrocytes was determined as described above. The percent of l-OHP partitioning in plasma and erythrocytes at each time point was calculated using the following formula:

$$\%\text{l-OHP partitioning} = \frac{\%\text{ dose of l-OHP in plasma or erythrocytes}}{\%\text{ dose of l-OHP in whole blood}}$$

2.6. Mouse dorsal air sac (DAS) model

The mouse DAS model was developed according to the method described by Nakamura et al. [29,30] with minor modification. Briefly,

Table 1
In vitro retention of l-OHP in PEG-coated cationic liposomes or PEG-coated neutral liposomes

Formulation		Retention of l-OHP (%)			
		1 h	3 h	6 h	24 h
PEG-coated cationic liposomes	50% Plasma	89.10	81.54	73.09	61.86
	5% Dextrose	99.70	94.50	88.90	85.16
PEG-coated neutral liposomes	50% Plasma	92.55	84.01	77.47	64.72
	5% Dextrose	97.82	97.80	89.45	83.63

Retention of l-OHP was determined at different times during incubation with the formulation in either 50% plasma or 5% dextrose at 37 °C.

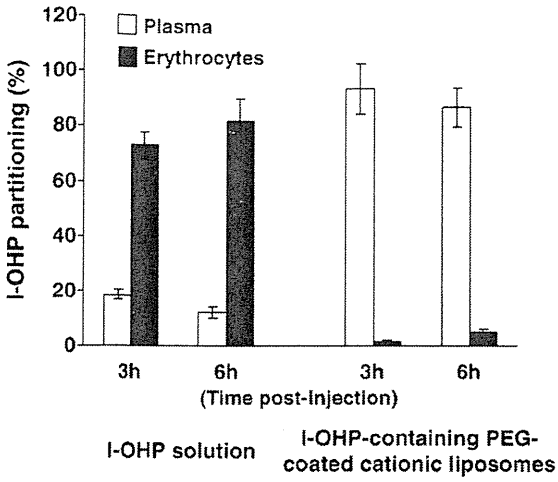

Fig. 1. Partitioning of I-OHP encapsulated in PEG-coated cationic liposomes into erythrocytes. Mice received intravenous injection with either free I-OHP solution or I-OHP-containing PEG-coated cationic liposomes. After 3 or 6 h injection, blood was collected, and the amount of I-OHP in plasma and erythrocytes was determined. Data are presented as the percentage of I-OHP partitioning in injected I-OHP dose. Data represents the mean±S.D. (n=3).

a chamber, which was prepared by covering both sides of a Millipore ring (10 mm diameter, 3 mm thickness) with Millipore filters (0.45-μm pore size), was filled with a suspension of B16BL6 tumor cells (1×10^7 cells) in 0.18 ml of DMEM. The chamber was then implanted into the subcutaneous dorsal air sac created by subcutaneous injection of 10 ml of air in anesthetized (25 mg/kg pentobarbital, i.p.) male ddY mice. At different days after chamber implantation, the animals were sacrificed and the skin was removed. The implanted chambers were removed from the subcutaneous fascia of the animals, and a black ring with the same inner diameter as that of the Millipore ring was placed at the same site. The angiogenic response, indicated by the formation of zigzag-shaped blood vessels, was observed under dissecting microscope (STeREO Lumar. V12, Zeiss, Germany).

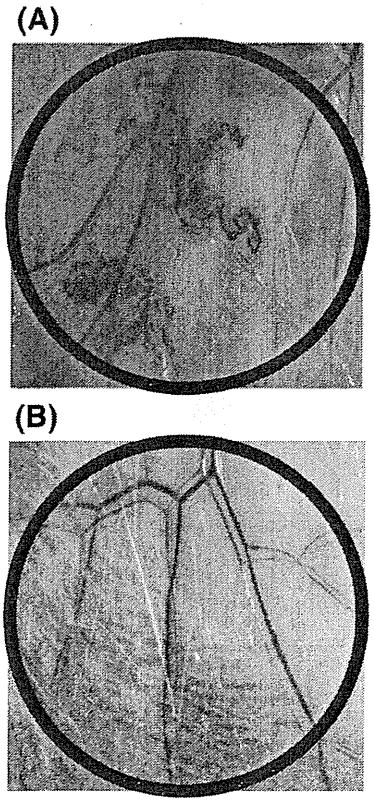

Fig. 2. Angiogenesis in the mouse DAS model. (A) Photograph of skin area attached to a chamber containing tumor cells (positive control). (B) Photograph of skin area attached to a chamber containing only DMEM (no tumor cells, negative control). 8x magnification.

2.7. Intracutaneous distribution of DiI-labeled liposomes

To induce neo-vascularization, a chamber containing tumor cells was implanted in the dorsal skin of the mouse. Five days later, DiI-labeled liposomes (no I-OHP, 45 mg total lipid/ mice) were intravenously administered. Eight hours later, the animal was sacrificed, and then the back-skin was removed. The area attached to the chamber was observed under the fluorescence microscope (STeREO Lumar. V12, Zeiss, Germany) to detect the accumulation of the liposomes in the newly formed vessels.

2.8. Evaluation of the anti-angiogenic effect of various I-OHP formulations

The *in vivo* anti-angiogenic activity of different I-OHP formulations was evaluated by using the DAS assay as follows.

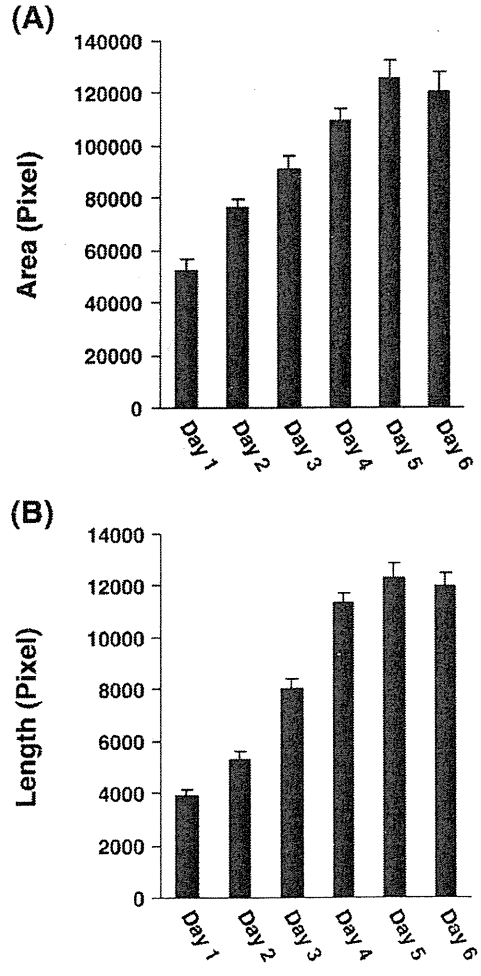

Fig. 3. Characterization of the mouse DAS model. Tumor-induced angiogenesis was evaluated sequentially from day 1 to day 6 post-chamber implantation. (A) represents the capillary network area of newly formed vessels. (B) represents the length of newly formed vessels. The values represent the mean±S.D. (n=3).

Experiment 1: Mice carrying the implanted chambers were treated with an intravenous injection of l-OHP encapsulated in PEG-coated cationic liposomes (5 mg l-OHP/kg, 45 mg total lipid/mouse) once on day 1, 2, 3 or 4 after chamber implantation. Mice carrying an implanted chamber and receiving no l-OHP treatment served as positive controls. Mice carrying an implanted chamber containing DMEM instead of tumor cells and receiving no l-OHP treatment served as negative controls. On day 5 after chamber implantation, angiogenesis was assessed by determining the dense capillary network area and length of angiogenic vessels in the area attached to the chamber using an Angiogenesis Image Analyzer (version 2, Kurabo).

Experiment 2: Mice (n=20) carrying implanted chambers containing tumor cells were divided into four groups. The first group received l-OHP-containing PEG-coated cationic liposomes (5 mg l-OHP/kg, 45 mg total lipid/mouse). The second group received "empty" (no drug) PEG-coated cationic liposomes (45 mg total lipid/mouse). The third group received l-OHP-containing PEG-coated neutral liposomes (5 mg l-OHP/kg). The last group received l-OHP solution (5 mg l-OHP/kg). All groups received the treatment via tail vein on the third day after chamber implantation. The angiogenesis was assessed as described above.

2.9. Statistical analysis

All values were expressed as the mean ± S.D. Statistical analysis was performed with the analysis of variance (ANOVA) test using GraphPad software (GraphPad Software, CA, USA). The level of significance was set at $p<0.05$.

3. Results

3.1. Characterization of liposomes

The size and zeta potential of l-OHP-containing liposomes were determined. The size of PEG-coated cationic liposomes was 250 ± 10 nm and the zeta potential was 11.24 ± 0.7 mV. The size of PEG-coated neutral liposomes (control liposomes) was 245 ± 6 nm and the zeta potential −6.9 ± 0.9 mV. The encapsulation efficiency of l-OHP was 25.4% for PEG-coated cationic liposomes and 22.0% for PEG-coated neutral liposomes.

Following storage in 5% dextrose at 4 °C for 4 weeks, the particle size of both formulations was changed slightly; 257 ± 17 nm for PEG-coated cationic liposomes and 249 ± 15 nm for PEG-coated neutral liposomes. This suggests that both formulations were stable in terms of size distribution during storage at 4 °C at least for 4 weeks.

3.2. In vitro stability of l-OHP liposomal formulations

We examined the retention of l-OHP in the liposomes upon incubation in 5% dextrose at 4 °C for up to 1 week. More than 80% of the encapsulated l-OHP still remained inside PEG-coated cationic liposomes and PEG-coated neutral liposomes (not shown). Then, the retention of the encapsulated l-OHP was investigated upon incubation in either 5% dextrose or 50% mouse plasma at 37 °C. As shown in Table 1, no remarkable difference was observed on the l-OHP retention between both liposomes, although 35–40% of encapsulated l-OHP was released following 24 h incubation. Moreover, it was shown that mouse plasma enhanced release rate of l-OHP from the liposomes, as

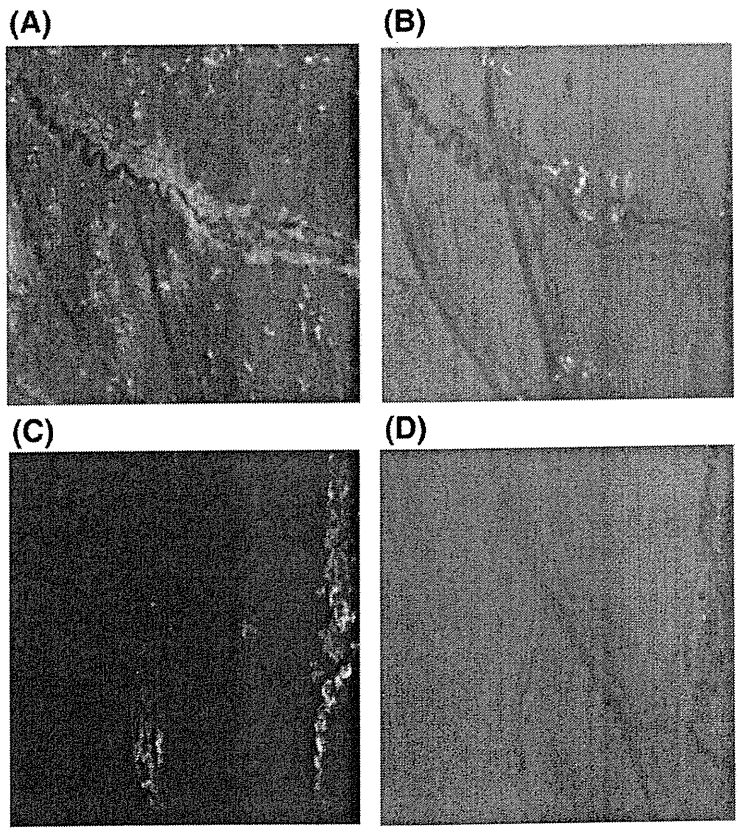

Fig. 4. Selectivity of PEG-coated cationic liposomes to newly formed blood vessels in the DAS model. (A) Skin area attached to a chamber 8 h after intravenous administration of DiI-labeled PEG-coated neutral liposomes observed by fluorescence microscopy. (B) Same area as in (A) under normal light. (C) Skin area attached to a chamber 8 h after intravenous administration of DiI-labeled PEG-coated cationic liposomes as seen by fluorescence microscopy. (D) Same area as in (C) under normal light. Each photograph is a representative example of at least 5 replicate experiments. 20x magnification.

compared with 5% dextrose. It appears that plasma proteins induce the leakage of l-OHP from both liposomes.

3.3. Partitioning of liposomal l-OHP into erythrocytes

The extent of partitioning of either free l-OHP or l-OHP encapsulated in PEG-coated cationic liposomes into erythrocytes was investigated at 3 and 6 h after intravenous injection of either free l-OHP solution or l-OHP encapsulated in PEG-coated cationic liposome. As l-OHP solution was injected, l-OHP was extensively taken up by erythrocytes (73.05% and 81.95% dose at 3-hour- and 6-hour post injection, respectively) and a small free fraction was available in plasma (Fig. 1). On the other hand, for l-OHP encapsulated in PEG-coated cationic liposomes, more than 90% dose of l-OHP was detected in plasma at each time point, while a little l-OHP (less than 10% dose) was taken up by erythrocytes (Fig. 1). These observations suggest that l-OHP-containing PEG-coated cationic liposomes were stable in blood circulation.

3.4. Characterization of DAS model

We first determined whether the DAS model induces *in vivo* angiogenesis. Newly formed microvessels having a zigzag-shape were abundantly produced as a result of the implantation of the tumor cells-containing chamber (Fig. 2A). Upon the implantation of chambers containing no tumor cells (negative controls) minimal angiogenesis was induced (Fig. 2B). This indicates that tumor cells, not the experimental manipulation and subsequent healing process, evoke a significant angiogenic response.

We then determined the optimal day for evaluating the angiogenic response induced by implantation of the tumor cells-containing chamber. As shown in Fig. 3A and B, the angiogenic response, as indicated by the dense capillary network area and length of angiogenic vessels, increased day by day and reached a maximum level on the fifth day post-chamber implantation. We therefore decided day 5 post-chamber implantation as a standard time point for evaluating angiogenesis in all subsequent experiments.

3.5. Selectivity of PEG-coated cationic liposome targeting to angiogenic blood vessels in the DAS model

The selectivity of PEG-coated cationic liposomes for the newly formed vessels was investigated in the DAS model. Eight hours after intravenous injection, control liposomes (PEG-coated neutral liposomes) had extravasated extensively into the interstitium in the skin, presumably through the leaky vasculature (Fig. 4A and B). By contrast, the PEG-coated cationic liposomes showed avid association with the newly formed vessels without any extravasation into the skin interstitium (Fig. 4C and D). No such accumulation of cationic liposomes was observed in the skin area attached to chambers containing only DMEM (data not shown). These observations indicate that the cationic liposomes possess selectivity to angiogenic vessels.

3.6. In vivo anti-angiogenic effect of l-OHP-containing PEG-coated cationic liposomes

The *in vivo* anti-angiogenic activity of l-OHP-containing PEG-coated cationic liposomes was investigated in the DAS assay. The l-OHP preparation was intravenously administered on day 1, 2, 3 or 4 after chamber implantation and the effect on neo-vascularization was examined microscopically on day 5. The photographs demonstrate that injection of cationic liposomes containing l-OHP on day 1 or 2 did

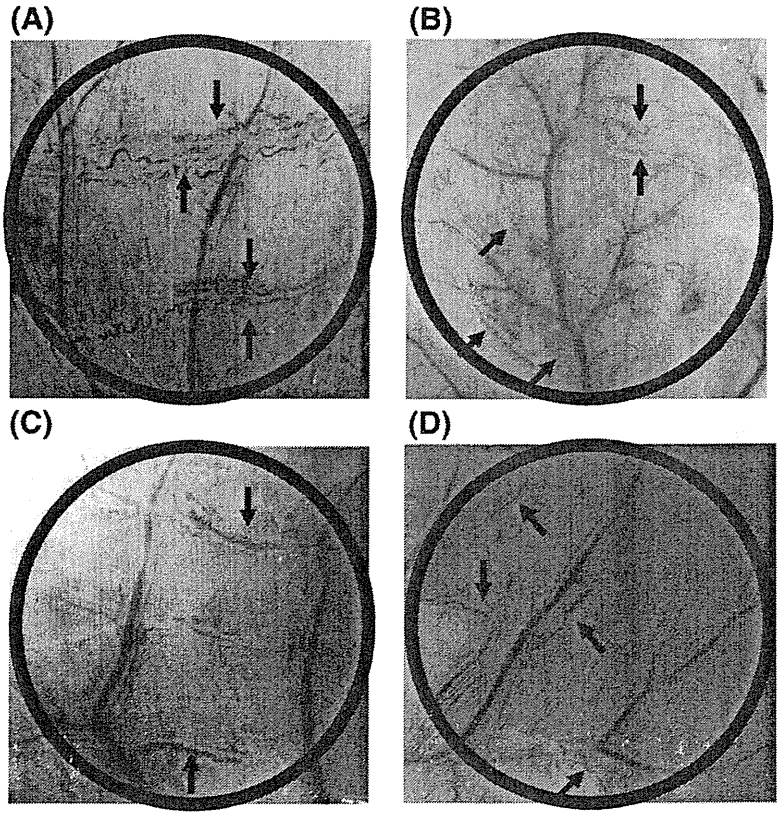

Fig. 5. Optical observation of the *in vivo* anti-angiogenic effect of l-OHP-containing PEG-coated cationic liposomes. Mice with an implanted chamber received l-OHP-containing PEG-coated cationic liposomes (5 mg l-OHP/kg) via tail vein on day 1 (A), 2 (B), 3 (C) or 4 (D) after chamber implantation. On day 5, the area of skin attached to the chamber was microscopically examined. Each photograph is a representative example of at least 5 replicate experiments. Arrow heads represent newly formed vessels. 8x magnification.

not suppress the angiogenesis (Fig. 5A and B), relative to the control group (Fig. 2A), while injection on day 3 or 4 strongly suppressed angiogenesis (Fig. 5C and D). A quantitative evaluation of the anti-angiogenic effect was obtained by determining the capillary network area and length of angiogenic vessels on the micrographs. Significant suppression of angiogenesis in terms of both area and length of vessels was observed in all treated groups when compared with the positive control (ANOVA, $p<0.05$) (Fig. 6A and B). Notably, the treatment on day 3 completely suppressed the angiogenesis to the negative control level. The results clearly indicate that l-OHP encapsulated in liposomes which are targeted to newly forming vessels can suppress angiogenesis with an efficacy that appears to depend on the time of administration.

3.7. Specificity of in vivo anti-angiogenic effect of l-OHP-containing PEG-coated cationic liposomes

On day 3 after chamber implantation, the efficacy of the *in vivo* anti-angiogenic effect of l-OHP-containing PEG-coated cationic liposomes was compared with that of free l-OHP, l-OHP-containing PEG-coated neutral liposomes and "empty" (no drug-containing) PEG-coated cationic liposomes (Fig. 7A and B). Free l-OHP and empty PEG-coated cationic liposomes caused only a slight suppression of angiogenesis. PEG-coated neutral liposomes induced a stronger suppression of angiogenesis than free l-OHP and empty PEG-coated cationic liposomes. PEG-coated cationic liposomes resulted in efficient anti-angiogenic activity superior to all other l-OHP formulations (ANOVA, $p<0.05$).

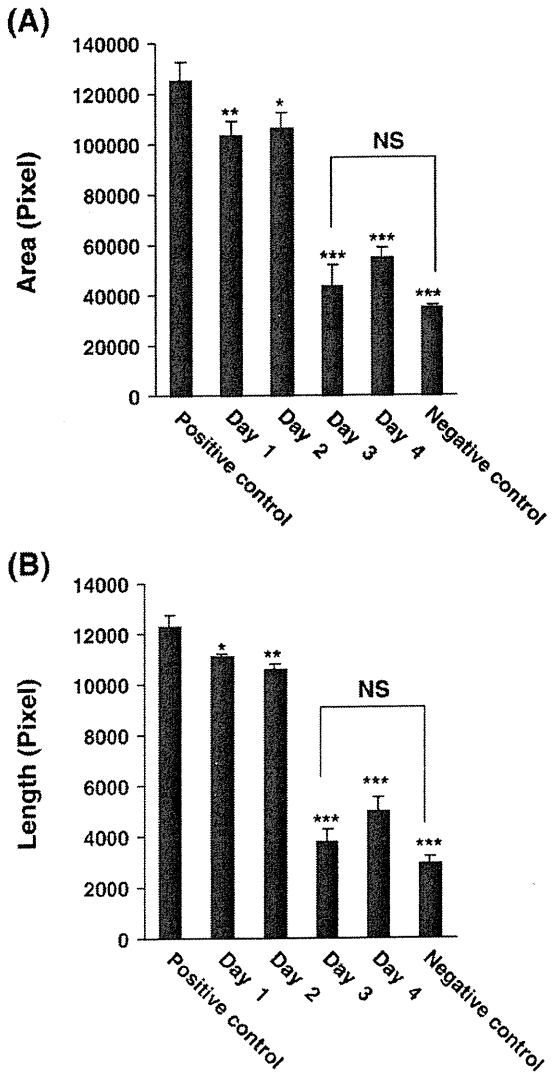

Fig. 6. Quantification of *in vivo* anti-angiogenic effect of l-OHP-containing PEG-coated cationic liposomes. The capillary network area (A) and length of newly formed vessels (B) in the area of skin attached to the chamber were measured on the basis of the photographs presented in Fig. 5. The values (n=5) represent the mean±S.D. * $p<0.05$, ** $p<0.01$, *** $p<0.005$ vs positive control; NS, not significantly different from the values at day 3 and negative control.

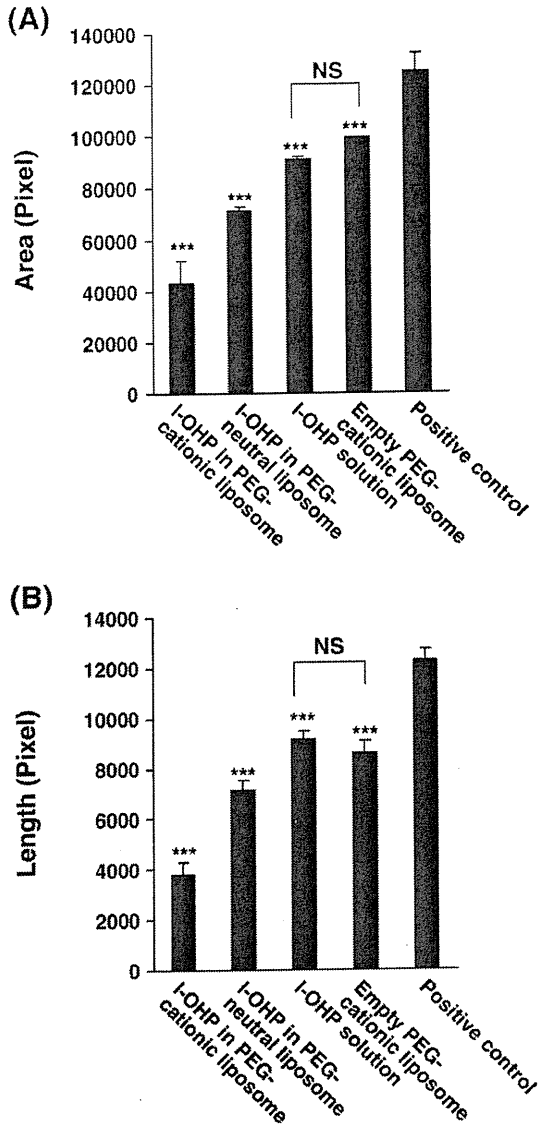

Fig. 7. Specificity of the in vivo anti-angiogenic effect of l-OHP-containing PEG-coated cationic liposomes. The anti-angiogenic effect of l-OHP-containing PEG-coated cationic liposome was compared with that of other formulations, i.e. free l-OHP, l-OHP encapsulated in PEG-coated neutral liposomes and "empty" (no drug containing) PEG-coated cationic liposomes. Mice with an implanted chamber received the formulations (5 mg l-OHP/kg, 45 mg total lipid/mouse) on day 3 after chamber implantation. On day 5, the skin area attached to the chamber was examined microscopically. The capillary network area (A) and length of newly formed vessels (B) on photographs taken were quantitatively determined. The values (n=5) represent the mean±S.D. The data for l-OHP-containing PEG-coated cationic liposomes and positive control were taken from the Fig. 6. *** $p<0.005$ vs positive control; NS, not significant.

4. Discussion

The purpose of this study was to develop a selective delivery system for l-OHP to areas of tumor-induced angiogenesis and to evaluate the

anti-angiogenic efficacy of l-OHP using the *in vivo* mouse DAS model. We chose for the use of cationic liposomes, because these have been reported to display a strong binding ability to tumor-derived angiogenic vascular endothelial cells due to the strong electrostatic adhesion between the cationic surface and the plasma membrane [32,33]. We modified the surface of cationic liposomes with $mPEG_{2000}$-DSPE, which makes it possible to prolong the circulation time of the liposomes by preventing interactions with the biological *in vivo* environment [34] thus enhancing their chance to gain access to the target angiogenic vessels. Our results indicate that the PEG-coated cationic liposomes we designed exhibit a selective accumulation/binding to the newly formed vessels (Fig. 4). In addition, no selective accumulation/binding of the liposomes to pre-existing blood vessels in the skin was observed (Fig. 4C and D). This points to an important difference in distribution of liposomes in blood vessels between normal tissues and tumor tissue, which may be exploited while attempting to achieve successful anti-angiogenic chemotherapy.

So far, free l-OHP has not been reported to suppress tumor-related angiogenesis, a crucial event in solid tumor growth [35,36]. This can probably be attributed to a low anti-tumor activity of l-OHP as a result of its high partitioning to erythrocytes and low accumulation in tumor tissues [6,7]. In the present study, a single injection of l-OHP encapsulated in PEG-coated cationic liposomes achieved complete suppression of angiogenesis in the DAS assay, while injection of either free l-OHP or l-OHP encapsulated in PEG-coated neutral liposomes only very slightly suppressed angiogenesis (Fig. 7). To the best of our knowledge, this is the first published observation of an anti-angiogenic effect of l-OHP. We assume that as a consequence of the selective delivery of l-OHP to the angiogenic vessels and its subsequent uptake by endothelial cells [13] the local concentration of the drug in/around proliferative vascular endothelial cells is increased. By contrast, the other l-OHP formulations are likely to suffer from high partitioning to erythrocytes (especially free l-OHP formulation) or massive distribution to the skin interstitium (especially PEG-coated neutral liposome formulation) (Fig. 4A), leading to an insufficiently high local drug concentration to exert a therapeutic effect.

In view of the results demonstrated in Figs. 5 and 6, it seems that the anti-angiogenic effect of l-OHP encapsulated in PEG-coated cationic liposomes is dependent on the time of drug administration. During the first 2 days after chamber implantation when the process of angiogenesis is not yet fully activated, the area to which the targeted liposomes can bind and thus site of action of the drug will be rather insignificant. At day 3 or 4 after the chamber implantation, however, when proliferation of endothelial cells is maximally activated, both the binding area of the liposomes and the site of action of the drug will be much larger. This is likely to be highly relevant to the clinical situation in case of tumor growth in that the efficacy of our l-OHP formulation is thought to depend on tumor progression which, in turn, strongly related to angiogenic-microvessel density.

Among various widely accepted methods used to evaluate the inhibition of angiogenesis [37], we selected the DAS model [29,30], a common and a reliable method, to evaluate the selectivity of PEG-coated cationic liposomes and the anti-angiogenic effects of liposome-encapsulated l-OHP. The DAS model is technically simple, provides a natural environment in which blood vessels and their tumor-induced formation can be studied. In addition, the model takes only about 5 days to develop and is therefore less time-consuming than the tumor-bearing mouse model, which takes more than 10 days. Therefore, the DAS model is a convenient and reliable method to effectively screen nanomolecular drug delivery systems targeting to tumor-induced neo-vascularization and evaluate the anti-angiogenic efficacy of the drug delivery system.

In recent years, l-OHP-based chemotherapy protocols, particularly l-OHP in combination with the infusion of 5-fluorouracil/leucovorin (FOLFOX), have emerged as the standard care in first- and second-line therapy of advanced-stage colorectal cancer [38,39]. In contrast to cisplatin, l-OHP has no renal toxicity, only mild hematological and gastrointestinal toxicity, while neurotoxicity is the dose-limiting toxicity [40,41]. This side effect has been described as a transient distal dysesthesia, enhanced by exposure to cold, and as a dose-related cumulative mild sensitive neuropathy [40,41]. The selective delivery of l-OHP to newly formed tumor-induced blood vessels as described here or to tumor tissues [6] by nanomolecular drug delivery systems raises the possibility of reducing the total l-OHP dose for the dosing regimen such as FOLFOX. This would improve the tolerance of patients and thereby improve the therapeutic efficacy as compared to the standard treatment protocols. Thus, the in vivo anti-angiogenic effect of our l-OHP formulation may lead to significant improvements in terms of survival rates and quality of life of patients with colorectal cancer.

Acknowledgments

We thank Dr. G.L. Scherphof for his helpful advice in preparing this manuscript. This study was supported, in part, by the Kobayashi Fund for Cancer Research and the Knowledge Cluster Initiative from Ministry of Education, Science and Technology.

References

[1] T. Nishikawa, N. Akiyama, K. Kunimasa, T. Oikawa, M. Ishizuka, M. Tsujimoto, S. Natori, Inhibition of in vivo angiogenesis by N-beta-alanyl-5-S-glutathionyl-3,4 dihydroxyphenylalanine, Eur. J. Pharmacol. 539 (2006) 151–157.
[2] T. Masuda, S. Ohba, M. Kawada, M. Osono, D. Ikeda, H. Esumi, S. Kunimoto, Antitumor effect of kigamicin D on mouse tumor models, J. Antibiot. (Tokyo) 59 (2006) 209–214.
[3] Y. Basaki, L. Chikahisa, K. Aoyagi, K. Miyadera, K. Yonekura, A. Hashimoto, S. Okabe, K. Wierzba, Y. Yamada, Gamma-hydroxybutyric acid and 5-fluorouracil, metabolites of UFT, inhibit the angiogenesis induced by vascular endothelial growth factor, Angiogenesis 4 (2001) 163–173.
[4] T. Tashiro, Y. Kawada, Y. Sakurai, Y. Kidani, Antitumor activity of a new platinum complex, oxalato (trans-l-1,2-diaminocyclohexane)platinum (II): new experimental data, Biomed. Pharmacother. 43 (1989) 251–260.
[5] K. Yonekura, Y. Basaki, L. Chikahisa, S. Okabe, A. Hashimoto, K. Miyadera, K. Wierzba, Y. Yamada, UFT and its metabolites inhibit the angiogenesis induced by murine renal cell carcinoma, as determined by a dorsal air sac assay in mice, Clin. Cancer Res. 5 (1999) 2185–2191.
[6] R. Suzuki, T. Takizawa, Y. Kuwata, M. Mutoh, N. Ishiguro, N. Utoguchi, A. Shinohara, M. Eriguchi, H. Yanagie, K. Maruyama, Effective anti-tumor activity of oxaliplatin encapsulated in transferrin-PEG-liposome, Int. J. Pharm. 346 (2008) 143–150.
[7] L. Pendyala, P.J. Creaven, In vitro cytotoxicity, protein binding, red blood cell partitioning, and biotransformation of oxaliplatin, Cancer Res. 53 (1993) 5970–5976.
[8] Y. Yu, L.G. Lou, W.P. Liu, H.J. Zhu, Q.S. Ye, X.Z. Chen, W.G. Gao, S.Q. Hou, Synthesis and anticancer activity of lipophilic platinum(II) complexes of 3,5-diisopropylsalicylate, Eur. J. Med. Chem. (2007).
[9] R.D. Hofheinz, S.U. Gnad-Vogt, U. Beyer, A. Hochhaus, Liposomal encapsulated anti-cancer drugs, Anticancer Drugs 16 (2005) 691–707.
[10] A.Z. Dudek, W.Z. Pawlak, M.N. Kirstein, Molecular targets in the inhibition of angiogenesis, Expert Opin. Ther. Targets 7 (2003) 527–541.
[11] K. Shimizu, N. Oku, Cancer anti-angiogenic therapy, Biol. Pharm. Bull 27 (2004) 599–605.
[12] J. Ye, Y. Li, T. Hamasaki, N. Nakamichi, T. Komatsu, T. Kashiwagi, K. Teruya, R. Nishikawa, T. Kawahara, K. Osada, K. Toh, M. Abe, H. Tian, S. Kabayama, K. Otsubo, S. Morisawa, Y. Katakura, S. Shirahata, Inhibitory effect of electrolyzed reduced water on tumor angiogenesis, Biol. Pharm. Bull. 31 (2008) 19–26.
[13] G. Thurston, J.W. McLean, M. Rizen, P. Baluk, A. Haskell, T.J. Murphy, D. Hanahan, D.M. McDonald, Cationic liposomes target angiogenic endothelial cells in tumors and chronic inflammation in mice, J. Clin. Invest. 101 (1998) 1401–1413.
[14] R.S. Kerbel, Tumor angiogenesis: past, present and the near future, Carcinogenesis 21 (2000) 505–515.
[15] N.M. Pandya, N.S. Dhalla, D.D. Santani, Angiogenesis—a new target for future therapy, Vasc. Pharmacol. 44 (2006) 265–274.
[16] T. Asahara, T. Takahashi, H. Masuda, C. Kalka, D. Chen, H. Iwaguro, Y. Inai, M. Silver, J.M. Isner, VEGF contributes to postnatal neovascularization by mobilizing bone marrow-derived endothelial progenitor cells, Embo J. 18 (1999) 3964–3972.
[17] D. Lyden, K. Hattori, S. Dias, C. Costa, P. Blaikie, L. Butros, A. Chadburn, B. Heissig, W. Marks, L. Witte, Y. Wu, D. Hicklin, Z. Zhu, N.R. Hackett, R.G. Crystal, M.A. Moore, K.A. Hajjar, K. Manova, R. Benezra, S. Rafii, Impaired recruitment of bone-marrow-derived endothelial and hematopoietic precursor cells blocks tumor angiogenesis and growth, Nat. Med. 7 (2001) 1194–1201.
[18] C.A. Staton, S.M. Stribbling, S. Tazzyman, R. Hughes, N.J. Brown, C.E. Lewis, Current methods for assaying angiogenesis in vitro and in vivo, Int. J. Exp. Pathol. 85 (2004) 233–248.

[19] S. Hussain, M. Slevin, S. Matou, N. Ahmed, M.I. Choudhary, R. Ranjit, D. West, J. Gaffney, Anti-angiogenic activity of sesterterpenes; natural product inhibitors of FGF-2-induced angiogenesis, Angiogenesis 11 (2008) 245–256.
[20] R. Kumar, J. Yoneda, C.D. Bucana, I.J. Fidler, Regulation of distinct steps of angiogenesis by different angiogenic molecules, Int. J. Oncol. 12 (1998) 749–757.
[21] T. Shibusa, N. Shijubo, S. Abe, Tumor angiogenesis and vascular endothelial growth factor expression in stage I lung adenocarcinoma, Clin. Cancer Res. 4 (1998) 1483–1487.
[22] L.S. Rosen, Clinical experience with angiogenesis signaling inhibitors: focus on vascular endothelial growth factor (VEGF) blockers, Cancer Control 9 (2002) 36–44.
[23] J. Folkman, The role of angiogenesis in tumor growth, Semin. Cancer Biol. 3 (1992) 65–71.
[24] M. Asano, A. Yukita, T. Matsumoto, S. Kondo, H. Suzuki, Inhibition of tumor growth and metastasis by an immunoneutralizing monoclonal antibody to human vascular endothelial growth factor/vascular permeability factor121, Cancer Res. 55 (1995) 5296–5301.
[25] B. Millauer, M.P. Longhi, K.H. Plate, L.K. Shawver, W. Risau, A. Ullrich, L.M. Strawn, Dominant-negative inhibition of Flk-1 suppresses the growth of many tumor types in vivo, Cancer Res. 56 (1996) 1615–1620.
[26] R.B. Campbell, D. Fukumura, E.B. Brown, L.M. Mazzola, Y. Izumi, R.K. Jain, V.P. Torchilin, L.L. Munn, Cationic charge determines the distribution of liposomes between the vascular and extravascular compartments of tumors, Cancer Res. 62 (2002) 6831–6836.
[27] S. Strieth, M.E. Eichhorn, B. Sauer, B. Schulze, M. Teifel, U. Michaelis, M. Dellian, Neovascular targeting chemotherapy: encapsulation of paclitaxel in cationic liposomes impairs functional tumor microvasculature, Int. J. Cancer 110 (2004) 117–124.
[28] A.V. Kalra, R.B. Campbell, Development of 5-FU and doxorubicin-loaded cationic liposomes against human pancreatic cancer: implications for tumor vascular targeting, Pharm. Res. 23 (2006) 2809–2817.
[29] M. Nakamura, Y. Katsuki, Y. Shibutani, T. Oikawa, Dienogest, a synthetic steroid, suppresses both embryonic and tumor-cell-induced angiogenesis, Eur. J. Pharmacol. 386 (1999) 33–40.
[30] T. Oikawa, M. Sasaki, M. Inose, M. Shimamura, H. Kuboki, S. Hirano, H. Kumagai, M. Ishizuka, T. Takeuchi, Effects of cytogenin, a novel microbial product, on embryonic and tumor cell-induced angiogenic responses in vivo, Anticancer Res. 17 (1997) 1881–1886.
[31] G.R. Bartlett, Colorimetric assay methods for free and phosphorylated glyceric acids, J. Biol. Chem. 234 (1959) 469–471.
[32] T. Nomura, N. Koreeda, F. Yamashita, Y. Takakura, M. Hashida, Effect of particle size and charge on the disposition of lipid carriers after intratumoral injection into tissue-isolated tumors, Pharm. Res. 15 (1998) 128–132.
[33] Y. Takeuchi, K. Kurohane, K. Ichikawa, S. Yonezawa, M. Nango, N. Oku, Induction of intensive tumor suppression by antiangiogenic photodynamic therapy using polycation-modified liposomal photosensitizer, Cancer 97 (2003) 2027–2034.
[34] C. Allen, N. Dos Santos, R. Gallagher, G.N. Chiu, Y. Shu, W.M. Li, S.A. Johnstone, A.S. Janoff, L.D. Mayer, M.S. Webb, M.B. Bally, Controlling the physical behavior and biological performance of liposome formulations through use of surface grafted poly(ethylene glycol), Biosci. Rep. 22 (2002) 225–250.
[35] C.J. Gomer, Preclinical examination of first and second generation photosensitizers used in photodynamic therapy, Photochem. Photobiol. 54 (1991) 1093–1107.
[36] B.W. Henderson, T.J. Dougherty, How does photodynamic therapy work? Photochem. Photobiol. 55 (1992) 145–157.
[37] R.K. Jain, K. Schlenger, M. Hockel, F. Yuan, Quantitative angiogenesis assays: progress and problems, Nat. Med. 3 (1997) 1203–1208.
[38] A. de Gramont, A. Figer, M. Seymour, M. Homerin, A. Hmissi, J. Cassidy, C. Boni, H. Cortes-Funes, A. Cervantes, G. Freyer, D. Papamichael, N. Le Bail, C. Louvet, D. Hendler, F. de Braud, C. Wilson, F. Morvan, A. Bonetti, Leucovorin and fluorouracil with or without oxaliplatin as first-line treatment in advanced colorectal cancer, J. Clin. Oncol. 18 (2000) 2938–2947.
[39] C. Tournigand, T. Andre, E. Achille, G. Lledo, M. Flesh, D. Mery-Mignard, E. Quinaux, C. Couteau, M. Buyse, G. Ganem, B. Landi, P. Colin, C. Louvet, A. de Gramont, FOLFIRI followed by FOLFOX6 or the reverse sequence in advanced colorectal cancer: a randomized GERCOR study, J. Clin. Oncol. 22 (2004) 229–237.
[40] A. Grothey, Oxaliplatin-safety profile: neurotoxicity, Semin. Oncol. 30 (2003) 5–13.
[41] A. Pietrangeli, M. Leandri, E. Terzoli, B. Jandolo, C. Garufi, Persistence of high-dose oxaliplatin-induced neuropathy at long-term follow-up, Eur. Neurol. 56 (2006) 13–16.

Journal of Controlled Release 134 (2009) 194–200

Contents lists available at ScienceDirect

Journal of Controlled Release

journal homepage: www.elsevier.com/locate/jconrel

Synergistic antitumor activity of metronomic dosing of cyclophosphamide in combination with doxorubicin-containing PEGylated liposomes in a murine solid tumor model

Tatsuhiro Ishida *, Emi Shiraga, Hiroshi Kiwada

Department of Pharmacokinetics and Biopharmaceutics, Subdivision of Biopharmaceutical Science, Institute of Health Biosciences, The University of Tokushima, 1-78-1, Sho-machi, Tokushima 770-8505, Japan

ARTICLE INFO

Article history:
Received 5 September 2008
Accepted 18 November 2008
Available online 3 December 2008

Keywords:
Combination therapy
Metronomic chemotherapy
Liposomal anticancer drug
PEGylated liposome
Cyclophosphamide
Doxorubicin

ABSTRACT

Cyclophosphamide (CPA) and doxorubicin (DXR)-containing sterically stabilized liposomes (DXR-SL) have a proven clinical activity. We propose that a metronomic CPA dosing schedule enhances accumulation of DXR-SL in solid tumors, because it causes apoptosis in the endothelial cells of the growing tumor vasculature and thereby may increase the permeability of the tumor microvessels. To establish the validity of this hypothesis we investigated the therapeutic benefits of metronomic CPA dosing (p.o.) combined with DXR-SL (i.v.) in a Lewis lung carcinoma, subcutaneously growing in C57BL/6 mouse. The metronomic CPA dosing clearly promoted accumulation and subsequent deep diffusion of SL in the solid tumor as a result of rather a transient increase in the density of $CD31^+$-microvessels, which shows high permeability to SL. It appears that the enhancing effect of metronomic CPA dosing is strongly dependent on the dose of CPA as well as on the time at which the treatment was initiated. Our study indicates that the use of metronomic chemotherapy combined with nanocarriers may be of significant clinical and practical importance in treating intractable solid tumors.

1. Introduction

In conventional chemotherapy with anticancer agents, the therapeutic agent is usually administered in short courses of therapy using the maximum tolerated dose (MTD chemotherapy). MTD chemotherapy requires prolonged drug-free breaks between successive cycles of therapy due to toxicity [1]. As an elegant alternative approach, a novel chemotherapeutic regimen, metronomic chemotherapy, has been advocated in recent years [1–3] implying the frequent administration of an anticancer agent at doses significantly below the MTD. This approach, which clearly shows lower toxicity, without the need for prolonged drug-free breaks, may also have potential for antitumor strategies involving a secondary alternative mechanism, i.e. inhibition of tumor angiogenesis [1–3]. Among various anticancer agents, cyclophosphamide (CPA), a traditional alkylating agent, is most frequently used for metronomic chemotherapy [4,5]. At lower doses, CPA is thought to induce apoptosis in tumor endothelial cells, subsequent collapse of angiogenic vessels, and ultimately suppression of tumor growth [6].

Liposomes were one of the first nanoparticulate drug delivery systems to show increased delivery of low molecular weight anticancer agents to solid tumors. Liposomes with diameters in the range of 100 nm can accumulate in solid tumors via the enhanced permeability and retention (EPR) effect [7], which occurs when nanoparticulates extravasate from the circulation into tumors through gaps in the vasculature endothelium [8]. The ability of liposomes to localize in solid tumors via the EPR effect partly depends on their long circulating properties, which can be achieved by grafting polyethylene glycol (PEG) to the surface of the liposomes (sterically stabilized liposomes (SL)) [9]. Anticancer agents encapsulated in SL have shown increased efficiency and lower toxicity in treatment of solid tumors by achieving higher accumulation in tumor tissue but limited accumulation in healthy organs [10,11]. Doxorubicin-containing SL (DXR-SL), Doxil/Caelyx, has been approved for clinical use [12,13].

Given the apoptosis induction potency of CPA in endothelial cells of growing tumor vasculature [6], we propose that a metronomic CPA-dosing schedule will increase the permeability of tumor microvessels to DXR-SL, resulting in a further enhanced accumulation of DXR in solid tumors. This may raise the possibility of increasing the therapeutic efficacy of liposomal DXR as well as a reduction in the total DXR dose. The reduction of DXR dose may improve tolerance of

Abbreviations: Ab, antibody; CHOL, cholesterol; CPA, cyclophosphamide; DiI, 1, 1′-dioctadecyl-3, 3, 3′, 3′-tetramethylindocarbocyanine perchlorate; DXR, doxorubicin; DXR-SL, DXR-containing sterically stabilized liposome; EPR, enhanced permeability and retention; FBS, fetal bovine serum; FITC, fluorescein isothiocyanate; HEPC, hydrogenated egg phosphatidylcholine; $mPEG_{2000}$-DSPE, 1, 2-distearoyl-*sn*-glycero-3-phosphoethanolamine-*n*-[methoxy(polyethylene glycol)-2000]; MTD, maximum tolerated dose; PEG, polyethylene glycol; SL, sterically stabilized liposome.

* Corresponding author. Tel./fax: +81 88 633 7260.
E-mail address: ishida@ph.tokushima-u.ac.jp (T. Ishida).

0168-3659/$ – see front matter © 2008 Elsevier B.V. All rights reserved.
doi:10.1016/j.jconrel.2008.11.019

patients and thereby improve therapeutic efficacy as compared to the conventional DXR therapy. In this study we therefore determined the efficacy of the combination of two anticancer agents, i.e. CPA and DXR-SL, using Lewis lung carcinoma, subcutaneously growing in C57BL/6 mice, as a model. In addition, we examined if metronomic CPA dosing truly enhances accumulation of SL in solid tumors as a result of an interference with the formation of the tumor vasculature.

2. Materials and methods

2.1. Materials

Hydrogenated egg phosphatidylcholine (HEPC) and 1, 2-distearoyl-*sn*-glycero-3-phosphoethanolamine-*n*-[methoxy(polyethylene glycol)-2000] ($mPEG_{2000}$-DSPE) were generously donated by NOF (Tokyo, Japan). Doxorubicin (DXR), cholesterol (CHOL) and cyclophosphamide (CPA) were purchased from Wako Pure Chemical (Osaka, Japan). FITC (fluorescein isothiocyanate)-labeled rabbit anti-rat IgG heavy and light chain polyclonal antibody (Ab) was purchased from Abcam (Cambridge, UK). Rat monoclonal anti-mouse CD45 Ab was purchased from R&D systems (CA, USA). FITC-labeled rat monoclonal anti-mouse CD31 Ab was purchased from Millipore (MA, USA). DiI (1, 1′-dioctadecyl-3, 3, 3′, 3′-tetramethylindocarbocyanine perchlorate) was purchased from Invitrogen (Paisley, UK). All other reagents were of analytical grade.

2.2. Animals and tumor cell line

Male C57BL/6 mice, 5 weeks old, were purchased from Japan SLC (Shizuoka, Japan). The experimental animals were allowed free access to water and mouse chow, and were housed under controlled environmental conditions (constant temperature, humidity, and a 12-h dark–light cycle). All animal experiments were evaluated and approved by the Animal and Ethics Review Committee of the University of Tokushima.

Lewis lung carcinoma cells were maintained in DMEM (Wako Pure Chemical) supplemented with 10% heat-inactivated fetal bovine serum (FBS) (Japan Bioserum, Hiroshima, Japan), 10 mM L-glutamine, 100 U/mL penicillin and 100 μg/mL streptomycin in a 5% CO_2/air atmosphere at 37 °C.

2.3. Preparation of liposomes

SL was composed of HEPC/CHOL/$mPEG_{2000}$-DSPE (2/1/0.1 molar ratio). Liposomes were prepared using the thin-film hydration technique, as previously described [14,15]. DiI labeled liposomes were prepared by the addition of DiI to the lipid mixture (1% related to total lipid) before formulation of a thin-film layer. The mean diameter of the liposomes was approximately 100 nm, as determined using a NICOMP 370 HPL submicron particle analyzer (Particle Sizing System, CA, USA). The phospholipid concentration was determined by a colorimetric assay [16]. DXR was encapsulated into the liposomes by remote loading using an ammonium sulfate gradient, as previously described [17]. After loading DXR into the liposomes, unencapsulated DXR was removed using a Sephadex G-50 column in 25 mM HEPES buffered saline (pH 7.4). DXR-loading efficiency was >90%.

2.4. Tumor model and assessment of antitumor effect

Lewis lung carcinoma cells were grown to 80–90% confluence in a 10 cm culture dish, harvested by treatment with trypsin, and resuspended in DMEM containing 10% FBS. The cells (5×10^5) in 0.1 mL DMEM were injected subcutaneously into the left flank of C57BL/6 mice. Most tumors reached a volume of approximately 50 mm^3 at day 5 and 1000 mm^3 at day 12, respectively. Treatments described below were started at day 5 or day 12 after inoculating the tumor cells.

Xenograft tumors were measured externally every third day. A group in which the treatment was started at day 5 was monitored from day 5 until day 29. The other group, in which is treatment was started at day 12, was monitored from day 6 until day 30. Tumor volume was approximated by using the equation $vol=(a\times b^2)/2$, where vol is volume, a the length of the major axis, and b is the length of the minor axis. The index of tumor-growth suppression was calculated as follows: The group in which the treatments were started at day 5 was calculated with the formula; [{1 − (tumor growth of treated group on day 24)/(tumor growth of control on day 24)} × 100]. The group in which the treatments were started at day 12 was calculated with the formula; [{1 − (tumor growth of treated group on day 27)/(tumor growth of control on day 27)} × 100].

2.5. CPA and DXR-SL dosing schedules

Treatments described below were started at either day 5 or day 12 after inoculating the tumor cells as follows:

(1) *Conventional CPA-dosing.* Mice ($n=5$) received a total 3 doses of CPA (150 mg/kg per dose) administered subcutaneously every other day (total dose: 450 mg/kg, i.e., MTD) [6,15].
(2) *Metronomic CPA-dosing. Group A*; mice ($n=5$) received eight doses of CPA (20 or 60 mg/kg per dose) administered orally at 3-day intervals (total dose: 160 or 480 mg/kg). The treatment was started at day 5 after tumor-inoculation. *Group B*; mice ($n=5$) received six doses of CPA (20 or 60 mg/kg per dose) administered orally at 3-day intervals (total dose: 120 or 360 mg/kg). The treatment was started at day 12 after tumor-inoculation.
(3) *Conventional DXR-SL dosing. Group A*; mice ($n=5$) received eight doses of DXR-SL (1 mg/kg) intravenously at 3-day intervals (total dose: 8 mg/kg). The treatment was started at day 5 after tumor-inoculation. *Group B*; mice ($n=5$) received six doses of DXR-SL (1 mg/kg) intravenously at 3-day intervals (total dose: 6 mg/kg). The treatment was started at day 12 after tumor-inoculation.
(4) *Combination of CPA dosing with DXR-SL dosing. Group A*; mice ($n=5$) received eight doses of CPA (20 or 60 mg/kg per dose, total dose: 160 or 480 mg/kg) administered orally and eight doses of DXR-SL (1 mg/kg per dose, total dose: 8 mg/kg) administered intravenously at 3-day intervals. The treatment was started at day 5 after tumor-inoculation. *Group B*; mice ($n=5$) received six doses of CPA (20 or 60 mg/kg per dose, total dose: 120 or 360 mg/kg) administered orally and six doses of DXR-SL (1 mg/kg per dose, total dose: 6 mg/kg) administered intravenously at 3-day intervals. The treatment was started at day 12 after tumor-inoculation.

2.6. $CD31^+$ microvessel density in the tumor following CPA treatment

To evaluate the effect of metronomic CPA-dosing on the density of newly formed vessels in the tumor, the tumor was removed at either day 6, 7, 8, 9, 10, 11 or 12 after tumor-inoculation from the mice orally treated with *metronomic CPA dosing (Group A)*. The tumors were excised and snap-frozen in OCT compound (Sakura Fintechnical, Tokyo, Japan) by dry-iced acetone. Frozen samples were cut into sections of 10-μm thickness in a cryostat (Leica Microsystems, Solms, Germany), mounted on a glass slide and dried in air. The samples were sequentially fixed by incubation in cold acetone, 1:1 acetone/chloroform and cold acetone for 5 min (each treatment), washed with PBS (pH 7.4) and blocked with 5% BSA in PBS for 30 min at room temperature. After washing with PBS, samples were incubated overnight with FITC-labeled rat anti-mouse CD31 at 4 °C. After washing with PBS, the number of microvessels was determined by fluorescence microscopy (Axioimager A1, Zeiss, Oberkohen, Germany). The microvessel density was evaluated according to the method previously demonstrated with minor modification [34].

2.7. Intratumoral distribution of fluorescence-labeled liposomes

To evaluate the effect of CPA dosing on intra-tumoral distribution of intravenously injected SL, DiI-labeled SL (5 mg phospholipids/kg) were injected either on day 5 or day 11 after tumor inoculation, into the mice orally treated with different doses of CPA (20 or 60 mg/kg). Mice were sacrificed 24 h after the SL injection, and tumors were excised and snap-frozen in OCT compound by dry-iced acetone. Frozen samples were cut into sections of 10-μm thickness in a cryostat (Leica Microsystems, Solms, Germany), mounted on a glass slide and dried in air. Samples were directly observed by using a fluorescence microscopy (Axioimager A1) to evaluate the intratumoral distribution of liposomes. After the observation, the samples on the glass slide were stained with anti-mouse CD31 Ab as described above.

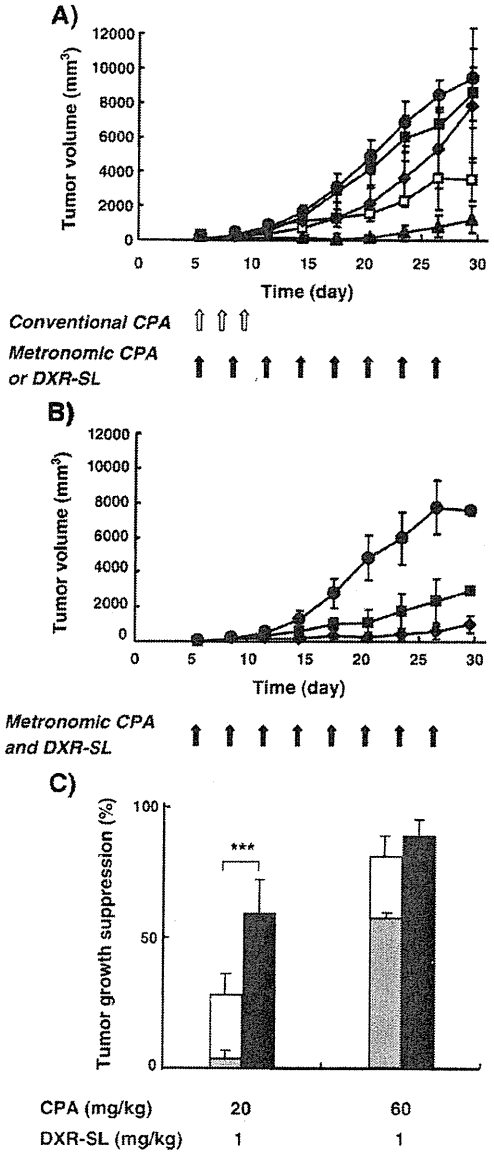

Fig. 1. Comparison of monotherapy and combination therapy with CPA and DXR-SL in early-stage solid tumor growth. (A) Monotherapy: Control (●), conventional CPA dosing (MTD) (▲), CPA (20 mg/kg) (■), CPA (60 mg/kg) ( ), DXR-SL (1 mg/kg) (◆). (B) Combination therapy: Control (●), CPA (20 mg/kg) plus DXR-SL (1 mg/kg) (■), CPA (60 mg/kg) plus DXR-SL (1 mg/kg) (◆). (C) Index of tumor-growth suppression: The bars indicate the index of tumor-growth suppression by monotherapies at different doses of CPA (gray bar) and DXR-SL (white bar), and by combination therapy by CPA plus DXR-SL (filled bar). The data represent mean±S.D. ($n=5$). ***, $p<0.005$.

2.8. Toxicity assessment

To avoid the influence of tumorigenesis on toxicity assessment, normal C57BL/6 mice were used for toxicity assessment [15]. Mice received eight cycles of CPA or DXR-SL treatment with 3-day intervals. One cycle consisted of either oral administration of CPA (20 or 60 mg/kg) or intravenous injection of DXR-SL (1 mg/kg). After treatment was initiated, body weight was measured every third day.

Total number of white blood cell (WBC) was determined according to the method previously reported [5]. Blood was collected from a different set of mice via retro-orbital puncture on day 6, 10, 15 and 24 after treatment was begun. After washing with cold PBS twice by centrifugation for 5 min at 300 ×g and 4 °C, blood cells were blocked with 1% BSA in PBS for 15 min at room temperature and then incubated with primary Ab (rat monoclonal anti-mouse CD45 Ab) for 30 min. After washing with cold PBS, samples were incubated for an additional 30 min with secondary Ab (FITC-labeled rabbit anti-rat IgG heavy- and light-chain polyclonal Ab). WBC number was determined using flow cytometry (Guava EasyCyte Mini System, GE Healthcare, CA, USA).

2.9. Statistics

All values are expressed as the mean±S.D. Statistical analysis was performed with a two-tailed unpaired t test using GraphPad InStat software (GraphPad Software, CA, USA). The level of significant was set at $p<0.05$.

3. Results

3.1. Antitumor effect of combined therapy

We elucidated whether metronomic CPA-dosing can promote the efficacy of DXR-SL thus achieving a synergistic antitumor effect without severe adverse effects. When treatment began on day 5 after tumor inoculation, monotherapy with CPA (20 mg/kg) or DXR-SL (1 mg/kg) showed very little antitumor effect (Fig. 1A). At higher dose (60 mg/kg), monotherapy with CPA induced significant antitumor effect, but the effect was lower than that of conventional CPA dosing (MTD) (Fig. 1A). Combination of metronomic CPA-dosing (20 or 60 mg/kg) with DXR-SL (1 mg/kg) achieved a marked antitumor effect (Fig. 1B), the higher CPA dose producing a stronger antitumor effect in combination with DXR-SL. The index of tumor suppression is presented in Fig. 1C. The data indicate that the combination of the metronomic *lower dose* CPA-dosing (20 mg/kg) with DXR-SL (1 mg/kg) produced a synergistic antitumor effect, whereas the combination of metronomic *higher dose* CPA-dosing (60 mg/kg) with DXR-SL (1 mg/kg) produced an additive effect.

We extended our study of the combination chemotherapy to larger tumors (approximately 1000 mm^3), 12 days after inoculation. Monotherapy with DXR-SL showed almost no antitumor effect (Fig. 2A). Monotherapy with the *higher dose* CPA (60 mg/kg) showed a slight antitumor effect, while monotherapy with the *lower dose* CPA (20 mg/kg) showed almost no antitumor effect (Fig. 2A). Combination of *high dose* CPA (60 mg/kg) with DXR-SL (1 mg/kg) achieved a substantial antitumor effect (Fig. 2B). By contrast, combination of the *lower dose* CPA (20 mg/kg) with DXR-SL (1 mg/kg) did not show any antitumor effect. The index of tumor suppression is presented in Fig. 2C. The combination *higher dose* CPA (60 mg/kg) and DXR-SL (1 mg/kg), produced a synergistic effect against the larger tumor.

3.2. Density of $CD31^+$ microvessels in tumors treated with metronomic CPA dosing

The density of $CD31^+$ microvessels in the tumor was determined from fluorescence microscopy images of four to five tumors (Fig. 3).

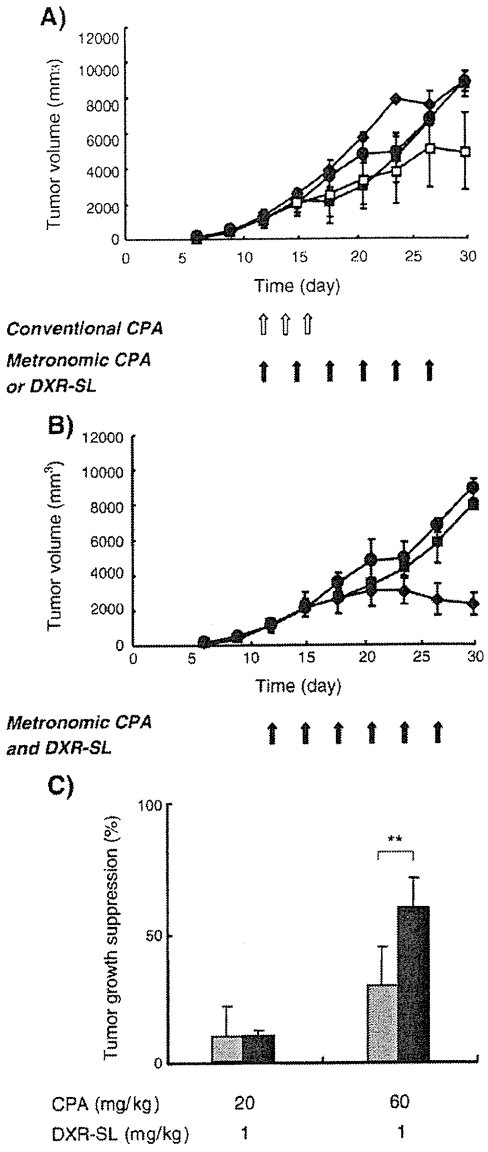

Fig. 2. Comparison of monotherapy and combination therapy with CPA and DXR-SL in late-stage solid tumor growth. (A) Monotherapy: Control (●), CPA (20 mg/kg) (■), CPA (60 mg/kg) (□), DXR-SL (1 mg/kg) (◆). (B) Combination therapy: Control (●), CPA (20 mg/kg) plus DXR-SL (1 mg/kg) (■), CPA (60 mg/kg) plus DXR-SL (1 mg/kg) (◆). (C) Index of tumor-growth suppression: The bars indicate the index of tumor-growth suppression by monotherapies at different doses of CPA (gray bar) and DXR-SL (white bar). The white bars do not show up because monotherapy with DXR-SL had no significant therapeutic effect. ● represents combination therapy by CPA plus DXR-SL. The data represent mean±S.D. ($n=5$). **, $p<0.01$.

Sequential oral (metronomic) doses of CPA (20 mg/kg or 60 mg/kg) were given on day 5, 8 and 11 after tumor inoculation. One day after the start of the first treatment (on day 6 after tumor-inoculation), the density of $CD31^+$-microvessels was decreased only at the higher CPA dose (60 mg/kg). Interestingly, the densities tended to increase as of the second day after the first treatment (day 7) but this tendency vanished after the second treatment on day 8. The second treatment initially normalized the density of $CD31^+$-microvessels to control levels and then microvessel density started to increase again. The third treatment on day 11 did not normalize $CD31^+$-microvessel density on day 12.

The effect of metronomic CPA dosing on the density of $CD31^+$-microvessels was also checked in the larger tumors 12 days after inoculation (i.e., *metronomic CPA dosing, Group B*). No significant changes in tumor microvasculature were detected throughout day 13 to 19 after tumor inoculation (data not shown).

It is noteworthy that the density of $CD31^+$-microvessels in the control tumors (without treatment) tended to decrease in a time after tumor inoculation dependent manner (Fig. 3). This might be due to a difference in proliferation rate between tumor cells and endothelial cells, the aggressive tumor cells growing much faster than the endothelial cells.

3.3. Effect of CPA dosing on the distribution and accumulation of SL in the solid tumor

To gain more insight in the underlying mechanism of the synergistic antitumor effect observed in Figs. 1 and 2, we investigated the effect of CPA dosing on the accumulation and distribution of co-administered DiI-labeled SL in the tumor. Either on day 6 or 12 after tumor inoculation (one day before SL injection), the tumor sections were stained with FITC-labeled anti-CD31 Ab and examined for FITC (green) and DiI (red) fluorescence (Fig. 4A and B). The area density of DiI-labeled SL accumulated in the tumors was measured as the proportion of pixels having a fluorescence intensity value equal to or greater than the corresponding threshold on the basis of fluorescence microscopic digital images. The amount of SL in the tumor without treatment was set as control.

In the smaller tumors (on day 5; approximately 50 mm^3), the lower CPA dosing resulted in a markedly enhanced accumulation of SL in the tumor (Fig. 4A and C) and a far broader distribution of SL around the $CD31^+$ microvessels in the tumor (Fig. 4A). The higher CPA dose did not enhance the SL accumulation into the tumor as same as the lower dose did (Fig. 4A and C). In the larger tumors (on day 12; approximately 1000 mm^3), the CPA dosing resulted in enhanced accumulation of SL in the tumor (Fig. 4B and C) and a distribution of SL around the $CD31^+$ microvessels (Fig. 4B). The lower CPA dose enhanced the SL accumulation into the tumor relative to the higher dose (Fig. 4B and C). It appears that the lower CPA dose strongly affects the tumor vasculature and simultaneously induces extravasation of SL into the tumor tissue compared to the higher CPA dose (Fig. 4C). Also, the vasculature in the massively growing tumor appears to be much more sensitive to the CPA treatment than that in the matured tumor (Fig. 4A and B).

3.4. Toxicity of combination therapy

Because the presence of a tumor influences bone marrow function and because treatment of tumor-bearing mice with chemotherapeutic agents may unfavorably interfere with a correct interpretation of toxicity data, we determined the toxicity of the combination therapy of CPA and DXR-SL in non-tumor-bearing mice [15]. The toxicity of the

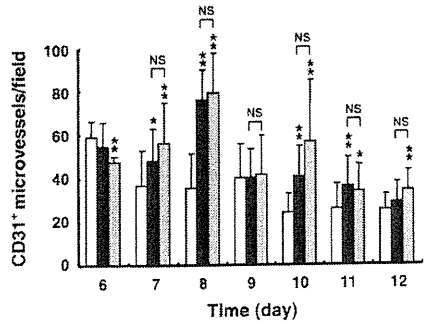

Fig. 3. CD31+-microvessel density in the tumor under a metronomic CPA-dosing schedule. Density of $CD31^+$ microvessels in the tumor was determined from fluorescence microscopic images taken from 4 to 5 tumors. CPA was orally administered on day 5, 8 and 11 after tumor-inoculation. Open column; control (without treatment). Filled column; CPA (20 mg/kg). Shaded column; CPA (60 mg/kg). *, $p<0.05$; **, $p<0.005$ versus Control. NS, not significant.

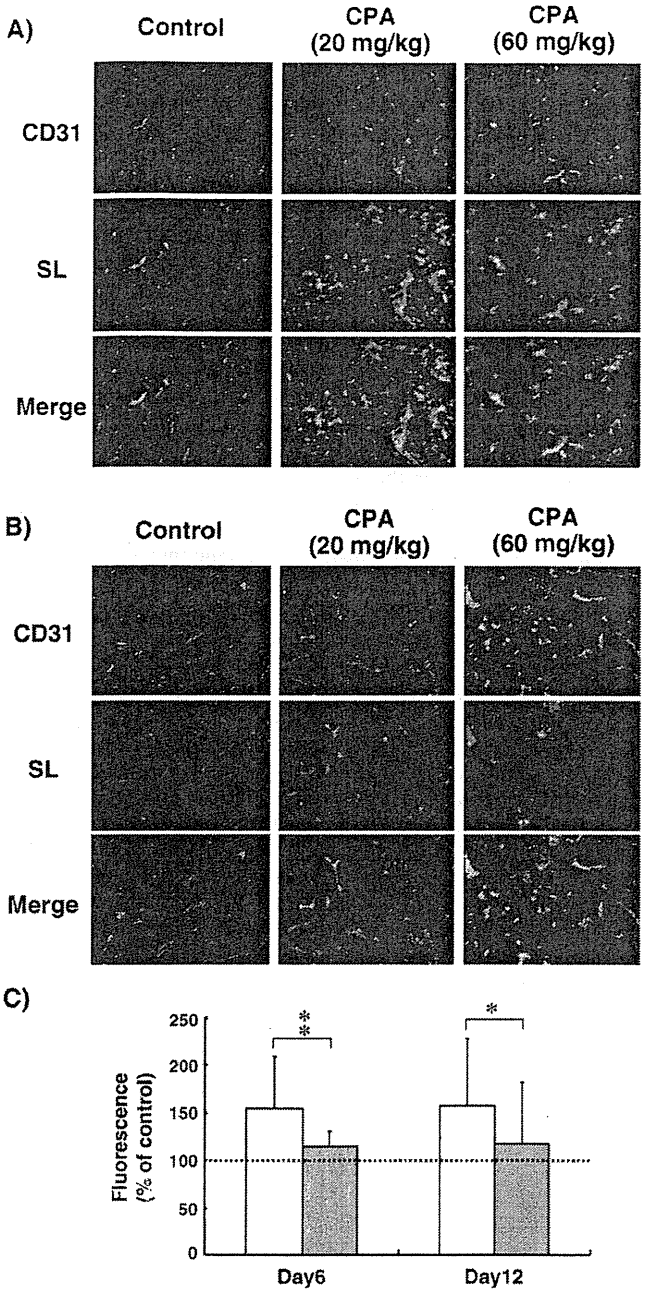

Fig. 4. Distribution of liposomes in tumor tissue. Immunofluorescence analysis of CD31$^+$ microvessels and fluorescence analysis of SL in the solid tumors (n=4–5). On day 5 (A) or day 11 (B) after tumor inoculation, CPA (20 or 60 mg/kg) was orally administered and subsequently DiI-labeled SL intravenously injected. 24 h later, cryosections of the tumor tissue were FITC-immuno-stained for the CD31$^+$ microvessels and then examined for FITC (green) and DiI (red) fluorescence. (C) Quantification of fluorescence intensity of DiI (representing SL). Open columns represent data from the tumor treated with CPA (20 mg/kg). Shaded columns represent data from the tumor treated with CPA (60 mg/kg). *, $p<0.05$; **, $p<0.01$ versus Control. Magnification, x100.

combination chemotherapy was estimated by measuring changes in body weight and WBC number.

A conventional CPA dosing schedule (MTD) led to a transient weight loss that was restored by the end of the cycle (Fig. 5A). As opposed to MTD of CPA, other monotherapeutic regimens did not cause weight loss but led to a mild delay in weight gain (Fig. 5A). The combination therapies did not cause any weight loss (Fig. 5B). However, the combination therapy with the higher CPA dose

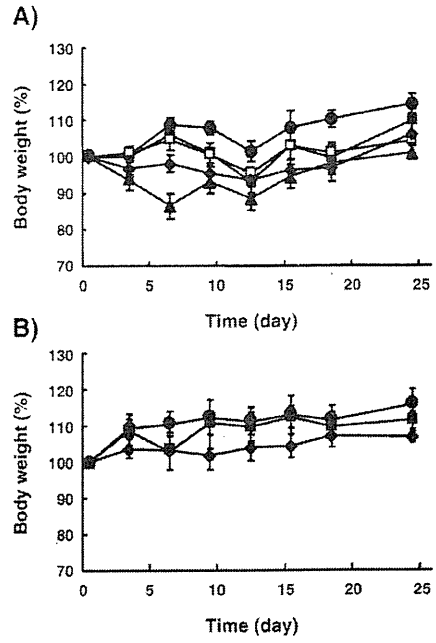

Fig. 5. Body weight change. (A) Monotherapy: Control (●), Conventional CPA dosing (MTD) (▲), CPA (20 mg/kg) at 3-day intervals (□), CPA (60 mg/kg) at 3-day intervals (■), DXR-SL (1 mg/kg) at 3-day intervals (◆). (B) Combination therapy: Control (●), CPA (20 mg/kg) and DXR-SL (1 mg/kg) at 3-day interval (■), CPA (60 mg/kg) and DXR-SL (1 mg/kg) at 3-day interval (◆). n=5 mice per group.

(60 mg/kg) led to suppression in weight gain (Fig. 5B). Tissue weights of treated mice (heart, lung, liver, kidney, and spleen) were not different from those of control mice (data not shown).

Two days after the last MTD CPA dose, WBC number was strongly reduced, followed by a strong overshoot at day 10 and restoration to normal levels by day 24 (Fig. 6A). Monotherapies also reduced the number of WBC, but the reduction was less dramatic than upon the

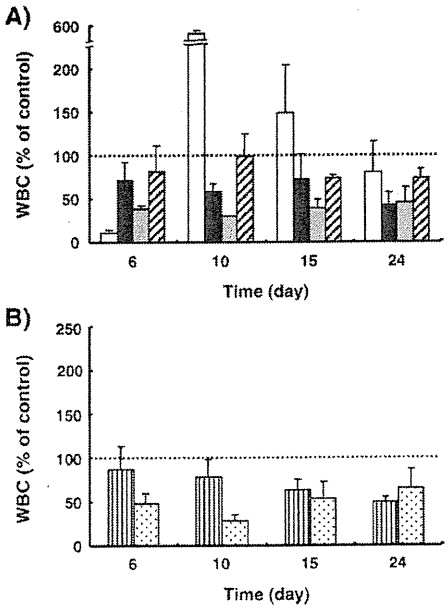

Fig. 6. Change in peripheral white blood cell (WBC) number relative to control (no treatment). (A) Monotherapy: Conventional CPA dosing (MTD) (white bars), CPA (20 mg/kg) at 3-day intervals (black bars), CPA (60 mg/kg) at 3-day intervals (grey bars), DXR-SL (1 mg/kg) at 3-day intervals (hatched bars). (B) Combination therapy: CPA (20 mg/kg) and DXR-SL (1 mg/kg) at 3-day interval (striped bars), CPA (60 mg/kg) and DXR-SL (1 mg/kg) at 3-day interval (dotted bars). n=5 mice per group.

conventional CPA dosing (MTD) (Fig. 6A). The combination regimens led to reduction in the number of WBC with no subsequent overshoot in WBC number (Fig. 6B). The reduction was similar to that observed for the metronomic CPA-dosing schedule. These findings indicate that adding DXR-SL to the metronomic CPA-dosing schedule does not increase bone marrow toxicity of CPA.

4. Discussion

The combination of a metronomic CPA dosing schedule with sequential injections of DXR-SL exerts synergistic antitumor activity in murine solid tumor model, as compared to administration of either treatment alone (Figs. 1 and 2), with no-overlapping toxic side effects (Figs. 5 and 6). It is generally accepted that long-circulating liposomes, such as sterically stabilized (PEGylated) liposomes (SL), accumulate in solid tumors via angiogenic blood vessels that have increased permeability [8] due to the so-called "EPR effect" [7]. Metronomic chemotherapy using CPA induces apoptosis in the endothelial cells of the growing tumor vasculature [6]. Therefore, we proposed that metronomic CPA dosing may increase the permeability of tumor microvessels to macromolecules during or before causing the collapse of microvessels, resulting in enhanced extravasation and subsequent accumulation of SL in the solid tumor. In this study, we confirmed that metronomic CPA dosing promotes enhanced accumulation of SL in the tumor tissue in a CPA-dose dependent manner (Fig. 4). This enhancing effect probably reflects the transient increase in density of microvessels in the tumor tissues (Fig. 3). Anti-angiogenic therapy causes tumor tissue hypoxia by diminishing blood flow, and the resulting hypoxia and acidification of the surrounding tissue can induce expression of angiogenic factors in the tumor [18]. Thus, metronomic CPA dosing might enhance subsequent angiogenesis in the tumor during drug-free intervals (for 2 days) (Fig. 3).

It is noteworthy that, in the metronomic CPA dosing, SL were found to penetrate deeply into the tissue (Fig. 4). The abnormalities in vessel and microenvironment of solid tumors may result in insufficient drug delivery and therapeutic efficacy [19]. Normalization of tumor vascular has been proposed to enhance drug delivery and improve tumor response to chemotherapy [20–22]. The metronomic CPA dosing may transiently normalize the tumor vasculature and microenvironment, because the therapy produces thrombospondin 1 (TSP1) [23] which is a well known endogenous inhibitor of angiogenesis [24]. Accompanied by vascular normalization, decreased interstitial fluid pressure would restore the pressure gradient across the blood vessel wall as well as tumor interstitium and thus, increase penetration of sequentially administered CPA in the tumor [22,25]. As a consequence, adequate CPA levels may be reached in the tumor tissue and lead to an enlargement in the tumor interstitial space into which SL is able to diffuse.

The density of $CD31^+$-microvessels in the treated tumors tended to decrease in a time after tumor-inoculation dependent manner, although the densities transiently increased in response to each CPA administration (Fig. 3). In addition, the combination chemotherapy with the *lower dose* CPA (20 mg/kg) and DXR-SL (1 mg/kg), led to a synergistic anticancer effect only when the therapy was applied in the early stage of tumor growth (day 5 after tumor inoculation) (Figs. 1 and 2). This suggests that metronomic CPA treatment-induced SL extravasation and diffusion would be transient and depend on the stage of tumor. Therefore, the timing, duration and extent of "enhanced extravasation window" towards SL are critical parameters of the metronomic CPA treatment. This strategy may extend to other types of anti-angiogenic and vasoactive agents. In fact, Kano et al. [26] recently reported that a low dose of transforming growth factor type I receptor (TβR-I) inhibitor promoted accumulation of nanocarriers (polymeric micelles) in a solid tumor. They showed that TβR-I inhibitor specifically increases the permeability of the tumor neovasculature by decreasing the degree of coverage of the endothelium without decreasing the number of endothelial cells, resulting in enhanced extravasation of the nanocarriers and an increase in therapeutic efficacy of the DXR-containing nanocarrier. In addition, ten Hagen and co-workers showed that co-administration of tumor necrosis factor-α (TNF-α) and liposomal DXR (DXR-SL) resulted in drug accumulation accompanied by pronounced tumor response in both rat and murine tumor models [27,28]. Accordingly, understanding the cellular and molecular mechanisms of the extravasation process of SL as observed in this study would be an important step towards the application and improvement of this strategy. Modification and control of the enhanced extravasation process may exhibit further synergistic effects by combination of liposomal anticancer agents and anti-angiogenic treatment.

We recently reported that the combination of a metronomic CPA dosing schedule with sequential injections of DXR-SL increases therapeutic efficacy in the murine lung metastatic B16BL6 melanoma model [15]. Under some dosage regimens, the therapeutic efficacy was accompanied by an increase in toxic side effects [15]. Therefore, we now improve the CPA regimen, i.e. reduction in each dose and total dose, and changing the dosage route. In addition, the dose of DXR-SL was set at 1 mg/kg, which was the low dose in our previous study [15]. Consequently, no overlapping toxic side effects were observed (Figs. 5 and 6). Originally, metronomic chemotherapy with CPA shows lower toxicity, because the dosage regimen refers to the frequent administration of CPA at relatively low, minimally toxic dose [1,6]. DXR is used to treat patients with sarcoma, lymphoma, and breast and ovarian carcinoma [29]. But its use is limited by potential cardiac toxicity, particularly at cumulative doses greater than 400 mg/m^2 [29]. Encapsulation of DXR in SL lowered its toxicity [12,13]. On the other hand, it has been reported that DXR-SL causes secondary cumulative adverse events in the later treatment cycle, namely stomatitis and skin-toxicity [12,30–33]. The novel dosage regimen, i.e. the metronomic CPA dosing plus DXR-SL, may overcome the limitations of DXR-SL, resulting in prolongation of survival and improvement on quality of life in patients. CPA and DXR-SL already have been approved for clinical use. Therefore, the combined regimen (metronomic CPA dosing plus DXR-SL) is considered to hold promise for approval in clinical use.

In conclusion, we show that metronomic CPA dosing augmented the accumulation of SL in a solid tumor by increasing the density of microvessels, which may have enhanced permeability towards 100-nm SL. This strongly correlated with an increased anti-tumor response. Because both CPA and DXR-SL (Doxil) are approved for clinical use, this regimen is considered to hold promise of clinical benefit in the treatment of intractable solid tumors.

Acknowledgements

We thank Dr. G.L. Scherphof for his helpful advice in writing the English manuscript. This study was supported in part by the Kobayashi Fund for Cancer Research and the Knowledge Cluster Initiative from Ministry of Education, Science and Technology.

References

[1] R.S. Kerbel, B.A. Kamen, The anti-angiogenic basis of metronomic chemotherapy, Nat. Rev. Cancer 4 (2004) 423–436.
[2] J. Gille, K. Spieth, R. Kaufmann, Metronomic low-dose chemotherapy as antiangiogenic therapeutic strategy for cancer, J. Dtsch. Dermatol. Ges. 3 (2005) 26–32.
[3] B. Laquente, F. Vinals, J.R. Germa, Metronomic chemotherapy: an antiangiogenic scheduling, Clin. Transl. Oncol. 9 (2007) 93–98.
[4] R. Munoz, S. Man, Y. Shaked, C.R. Lee, J. Wong, G. Francia, R.S. Kerbel, Highly efficacious nontoxic preclinical treatment for advanced metastatic breast cancer using combination oral UFT-cyclophosphamide metronomic chemotherapy, Cancer Res. 66 (2006) 3386–3391.
[5] Y. Shaked, U. Emmenegger, G. Francia, L. Chen, C.R. Lee, S. Man, A. Paraghamian, Y. Ben-David, R.S. Kerbel, Low-dose metronomic combined with intermittent bolus-dose cyclophosphamide is an effective long-term chemotherapy treatment strategy, Cancer Res. 65 (2005) 7045–7051.